3. SPIN-POLARIZED SUPERCURRENT IN PROXIMITIZED SINGLET SUPERCONDUCTOR – HALF-METALLIC MANGANITE NANOSTRUCTURES

V. Krivoruchko[1], V. Tarenkov[1]

Abstract

A common path to superconducting spintronics, superconducting magnonics, and topologically protected quantum computing relies on spin-triplet superconductivity. However, superconductors realizing spin-triplet *p*-wave pairing are not common in nature. While naturally occurring spin-triplet superconducting pairing is very exclusive, proximity effects in ferromagnet / superconductor heterostructures can overcome this limitation. That is why artificial nanostructures demonstrating equal-spin triplet superconductivity have attracted special interest as new functional materials. In this chapter, we present the results of experimental and theoretical investigations of proximitized nanocomposites based on half-metallic manganites – singlet *s*-wave or *d*-wave superconductors. The experimental data obtained, and theoretical reasoning give conclusive evidence that proximity induced long-range superconducting state in such hybrid structures can be qualitatively and quantitatively understood within the scenario of proximity induced *p*-wave spin-triplet superconductivity. It means that the superconductor–half-metallic manganites nanostructures are promising functional materials for superconducting spintronics, superconducting magnonics, and topologically protected quantum computing.

✉ Vladimir Krivoruchko
krivoruc@gmail.com

[1] O. O. Galkin Donetsk Institute for Physics and Engineering, National Academy of Sciences of Ukraine, Nauki Ave. 46, 03028 Kyiv, Ukraine

3.1 Introduction

Over past decades, one of the basic directions in the condensed matter physics has been search of materials for *superconducting spintronics*, *superconducting magnonics*, as well as materials with topologically protected quasiparticle excitations for a *quantum computer*.

Digital superconductive electronics is inherently faster at much less power dissipation than semiconductor analogue. That is why a superconducting version of the conventional spintronics – superconducting spintronics – has become the most attractive subject of spintronics in past decades [3.1–3.6]. The idea of combining superconductivity with spintronics and magnonics has focused on the net spin polarization of quasiparticles in superconductors – triplet Cooper pairs. Condensed materials with the spin-triplet superconducting pairing state will have great potential applications in the field of superconducting spintronics and magnonics and recent experimental demonstration of spin-polarized supercurrents in proximitized structures provides a guiding principle of the functional materials establishment. The field of superconducting spintronics and magnonics offers new concepts for spin transmission by combining superconducting phase coherence and magnetism [3.4, 3.7]. Spin-polarized supercurrent offers new ideas to carry information by spin instead of charge, leads to massive reductions in ohmic losses and support the development of novel spin-based devices. The exploration of superconducting spin currents opens fascinating potential for novel spintronic device concepts.

At the present time in the condensed matter physics a ‘second quantum revolution’ is carried out through the introduction of topology-originated concepts used to characterize physical states and properties of solids (see, e. g., reviews [3.8–3.11] and references therein). With the introduction of topology, the description of phase transitions and phases of the system expands and includes not only differentiating in terms of a local (Landau) order parameter, but also those characterized in terms of global quantities that are measured nonlocally and which endow the system with a global stability to perturbations. Topological state is a state of a matter characterized by nonzero topological number of the wave functions and nontrivial topological states of their quasiparticles. One of the promising motivations of topology-originated views in the condensed matter physics is searching for materials to create a quantum

computer. The most significant obstacles for successful realization of a quantum computer are the quantum decoherence, i. e., a loss of information from a system. In this regard, quantum computing, based on topologically protected excitations has been considered as an attractive solution for overcoming the related problems [3.12–3.16]. It processes quantum information in a nonlocal fashion, and in addition exploits the peculiarities of non-Abelian braiding statistics, allowing the performance of decoherence-free and fault-tolerant quantum logical operations [3.15]. In this standpoint, so-called Majorana fermions have been proposed as elementary building blocks of a topological quantum computing hardware [3.16].

Majorana fermions are fundamental particles originally proposed in 1937 by E. Majorana as a real solution to the Dirac equation. The Majorana fermion is a fermion that is its own antiparticle has no charge but can carry spin or heat. Among promising grounds for topologically protected non-Abelian excitations like Majorana fermion is a superconducting state. Topological superconducting states support topologically protected gapless Andreev bound states that are their own antiparticles, and which partially mimic the so-called zero mode Majorana fermions. Recently, a great effort has been put towards an unambiguous experimental detection of Majorana fermions in systems which, as expected, can be in the topological superconducting state (see, e. g., reviews [3.8–3.10] and references therein).

Though topological materials and their unusual properties are in a focus of modern experimental and theoretical research in condensed matter physics, beyond doubt, experimental identification / observation of Majorana quasiparticles is still absent. Materials having good prospects for the topological superconducting phase realization are those with the spin-triplet superconducting pairing state [3.10]. Indeed, in a *p*-wave superconductor (SC) Bogoliubov quasiparticles, $b_{\mathbf{k}\sigma} = uc_{\mathbf{k}\sigma} + vc_{-\mathbf{k}\sigma}^{+} = (u - v^{*})c_{\mathbf{k}\sigma} + (v^{*}c_{\mathbf{k}\sigma} + vc_{-\mathbf{k}\sigma}^{+})$, have both electron and hole components of equal spin projection, σ, and thus can possess the Majorana fermions properties. The task is to create necessary conditions when *p*-wave Bogoliubov quasiparticles are ‘forced’ to demonstrate their Majorana fermions characteristics, i. e., when $b_{\mathbf{k}\sigma} \rightarrow (v^{*}c_{\mathbf{k}\sigma} + vc_{-\mathbf{k}\sigma}^{+})$. Yet, SC realizing a spin-triplet *p*-wave pairing is not common in nature; Sr_2RuO_4 with the critical temperature $T_C \approx 1.5$ K being the only realistic candidate so far.

A way that overcomes this difficulty settles in artificially engineered topological materials. Artificially engineered topological superconductivity in SC-magnet hybrid structures are currently attracting attention, because, as expected, they represent one of the most promising platforms for realizing topological superconducting phases [3.10, 3.17–3.21]. Particularly, Choy *et al*. has proposed to create Majorana fermions by depositing a chain of magnetic nanoparticles on an *s*-wave superconducting substrate [3.17]. Chung *et al*. [3.18] consider the creation of spin-triplet superconductivity and topological phase in SC / half-metal heterostructures (a half-metal is a spin-polarized metal at the Fermi surface, *i. e.*, a metal for the majority spin and an insulator for the minority spin).

Superconducting phase needs cooling to quite low temperatures. For practical applications cooling with liquid helium is not adequate because the handling is too error prone. In this chapter, we discuss a promising way for creating artificial materials with a high-temperature triplet superconductivity. These are hybrid spin-singlet superconductors–half-metallic manganites nanostructures; in particular, nanocomposites of half-metallic manganites nanoparticles and *s*-wave or *d*-wave SCs. A key factor of these hybrid structures is *local high-temperature triplet superconductivity* of half-metallic manganites. The experimental evidence for the existence of latent (noncoherent) spin-triplet pairing in half-metal manganites is presented and conditions favoring their topological superconductivity are discussed. Our findings presented here are substantially based on the experimental results, especially obtained in Refs. [3.22–3.36], evidencing unconventional superconducting proximity effect in SC / half-metallic manganites hybrid structures.

Summing the above, a common path to superconducting spintronics, superconducting magnonics, and topologically protected quantum computing relies on spin-triplet superconductivity. While naturally occurring spin-triplet superconducting pairing is very exclusive, proximity effects in ferromagnet / superconductor heterostructures can overcome this limitation.

3.2 Coexistence of superconductivity and ferromagnetism, proximity effect

Ferromagnetic order and singlet superconductivity are incompatible, since in a ferromagnet (F) the exchange field H_{exc} splits conduction bands. In a typical metal ferromagnets the exchange energy is larger than the pairing energy of electrons in singlet Cooper pairs by orders of magnitude, so that only triplet amplitudes of the form $f^{tr}(\boldsymbol{r}) = g_1(\boldsymbol{r})|\uparrow\uparrow>$ or $f^{tr}(\boldsymbol{r}) = g_2(\boldsymbol{r})|\downarrow\downarrow>$ can be supported. That is why, when a metallic F is in contact with *s*-wave SC, *s*-wave Cooper pairs can penetrate into F layer by diffusing only over the small distance given by the superconducting penetration depth $\xi_F = (4\hbar D_F/H_{exc})^{1/2}$, here D_F is the diffusion coefficient of the conduction electrons in the F layer).

The incompatible nature of superconductivity and ferromagnetic order was confirmed in various materials and geometries. Yet, number of experimental facts point also that a physical interpretation of the proximity effect when Cooper pairs are broken by a strong exchange field H_{exc} in the F layer can be too simplified. Long-ranged proximity effects have been observed in a variety of ferromagnetic materials, including wires [3.37, 3.38], bi- and multilayers [3.39], half-metallic $La_{0.7}Ca_{0.3}Mn_3O$ [3.40] and CrO_2 [3.41], rare-earth metals with helical magnetic structure [3.42] *etc*. Coexistence of superconductivity and ferromagnetism close to the interfaces in hybrid SC/F systems leads to unusual and interesting phenomena. If a ferromagnet with a uniform exchange field is in a metallic contact with a SC, from a theoretical viewpoint, the base physics is well understood, and the proximity effect is described by considering the splitting of electronic bands of opposite spins [3.43]. The situation becomes more complicated when the magnetic structure is inhomogeneous. Theories [3.26, 3.44, 3.45] predict the appearance of a long-range proximity effect if there is a spatial variation of the magnetization in the F layer. In this case, the triplet component of anomalous correlations needs to be taken into consideration with a characteristic coherence length of $\xi_F = (\hbar D_F/2\pi T)^{1/2}$ that can be as large as ~100 nm at low temperatures (here T is the temperature; we choose $k_B = 1$). See, *e. g.*, the discussion in Ref. [3.5, 3.26, 3.45] and references therein.

Magnetic inhomogeneities may, in principle, be artificially generated in ferromagnets. Yet, existing technology cannot create them in a controlled way

at the SC/F interface with a nanoscale precision so that the most realistic scenario is to use a ferromagnet with given magnetic inhomogeneity. An interesting limit of systems with tunable inhomogeneity of the magnetic partner is SC/F nanocomposites. Being an experimentally accessible electronic system with controllable parameters, such heterostructures offer a unique testing ground for studying superconducting proximity effect in systems with an arbitrary length of magnetic disorder. Superconductivity in a granular mixture of superconductor-insulator films has been extensively studied, both experimentally and theoretically, in the framework of the percolation theory (see, e. g., Ref. [3.46]). The proximity effects in granular superconductor–normal-metal structures are also explored [3.47, 3.48]. Proximity effects in composites of a (nano)granular half-metal ferromagnet (hmF) and conventional *s*-wave or *d*-wave superconductors will be discussed in Sec. 3.4.2.

Equal-spin *p*-wave triplet Cooper pairs are immune to the exchange field and can propagate into ferromagnetic metals over the same long distance as singlet pairs into normal metals. However, superconductors realizing a spin-triplet *p*-wave pairing are not common in nature; Sr_2RuO_4 with $T_C = 1.5$ K being the only real candidate, so far. That is why artificial materials demonstrating *p*-wave superconductivity have attracted notable interest. A microscopic quantum mechanism on which the long-range triplet condensate induced in artificial materials is based on the Andreev reflection [3.49].

As is known, at energies below the superconducting gap, the charge transport through a normal nonmagnetic (N) metal been in contact with a SC is possible only due to the specific two-particle process, called Andreev reflection [3.49]. In the N metal, an incident electron above the Fermi energy E_F and an electron below E_F with the opposite spin are coupled together and transferred across the interface into the SC side, forming a singlet Cooper pair in the condensate. Simultaneously, an evanescent hole with opposite momentum and spin appears in the N metal. This implies the doubling of the normal-state conductance since two electrons are transferred across the interface into the SC region where they form a spin-singlet Cooper pair. Unlike this conventional Andreev reflection, a spin-active interface with interfacial spin-flip scattering also yields Andreev reflection with an equal spin of electrons and holes [3.5, 3.50], responsible for spin-triplet pair correlations, see Fig. 3.1. As

the Cooper pair's size is determined by the superconducting coherence length *s*-wave Cooper pairs extend on a coherence length from the interface SC/F into the F bulk and near the SC/F interface a singlet-triplet mixed Cooper pairs state is formed. (For more details the reader is referred, *e. g.*, to articles [3.5, 3.43, 3.45, 3.51]). The two phenomena, proximity effect and Andreev reflection are intertwined and cannot be discussed separately from each other. The superconducting proximity effect is evidence of the macroscopic quantum coherence and prove the macroscopic character of the Cooper pair wave function.

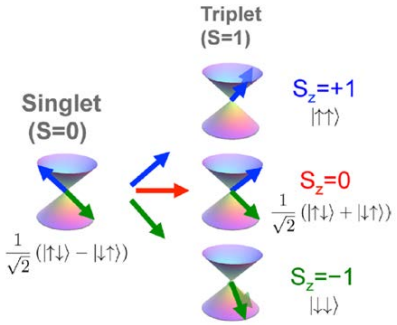

Fig. 3.1 – Andreev reflection at the SC/F interface. Adapted from Ref. [3.5]

Symmetry classification of Cooper pairs in superconductors. Note to avoid confusion, here and below we mean the *ordinary* triplet pairing. That is the Cooper pair wave function is even-spin, even-frequency, odd-momentum. An unconventional new type of superconducting pairing function (even-spin, even-momentum, odd-frequency) the so-called odd triplet pairing, was predicted theoretically [3.45], too. To date, it remains under question direct experimental verification of the odd-frequency symmetry Cooper pair wave function, and we will not consider this superconducting state below.

3.3 Ferromagnetic manganites, spin-polarization, and half-metallicity

Magnetic and transport properties of manganites $R_{1-x}A_xMnO_3$, where trivalent cations R^{3+} are substituted by divalent ones A^{2+}, are discussed in detail in reviews [3.52–3.54] Here we summarized the main physics and statements.

Bulk samples. The initial compound $RMnO_3$ has a perovskite structure. It is electrically homogeneous due to the single valence of the Mn^{3+} ion and below the Neel temperature $T_N \approx 130$ K exhibits an antiferromagnetic order. Compounds of the type $R_{1-x}A_xMnO_3$, where a divalent ion A^{2+} (= Ca, Sr, Ba, Pb, …) replaces the trivalent ion R^{3+}, are electrically inhomogeneous with a competition between different types of magnetic interactions among the Mn ions due to random positions of ions Mn^{3+} and Mn^{4+} having different ionic radii, charges, and spins. When the concentration of the A^{2+} ions exceed ~1/8, the material undergoes a transition to a ferromagnetic state with a metallic type of conductivity. The Curie temperature of the ferromagnetic state depends significantly on the extent of substitution and the difference in the ionic radii of the A^{2+} and La^{3+} ions. The highest value of Curie temperature, close to 360 K, is attained in the compound $La_{5/8}Sr_{3/8}MnO_3$. The ferromagnetic-paramagnetic transition itself appears to be close to a second order phase transition and the behavior of the system is described by critical indices corresponding (or close) to a three-dimensional Heisenberg ferromagnet. (The specific realization of the metal-insulator transition in manganites with colossal magnetoresistance caused by inhomogeneities in the electronic and magnetic states of the manganites near the Curie temperature is reviewed in Refs. [3.52–3.54]).

In terms of the traditional model proposed by Zener [3.55], magnetic and transport properties of the substituted manganites are generated by the so-called 'double-exchange' interaction. In brief, consider two cations Mn^{3+} and Mn^{4+} located at equivalent crystallographic positions and separated by an O^{2-} anion. The Mn^{4+} ion is in a t_{2g}^3 configuration and the Mn^{3+} ion is in a $t_{2g}^3 e_g^1$ configuration. Because of the large intra-atomic Hund coupling, the three electrons in the t_{2g} level form a localized spin S = 3/2. Due to the same Hund rule, the e_g electron on the Mn^{3+} ion has its spin aligned parallel to the localized spin of the ion. Since the positions of the Mn ions are equivalent, the $Mn^{3+} - O^{2-} - Mn^{4+}$ and $Mn^{4+} - O^{2-} - Mn^{3+}$ configurations are energetically equivalent, i. e., the ground state of the pair is degenerate. It is natural to expect a strong resonance coupling between the two configurations, which can be interpreted as a state of two Mn^{4+} cations with a generalized e_g-electron (or Mn^{3+} cations with a generalized hole). As an e_g-electron moves along the lattice it is energetically favorable that all the localized spins be parallel to one

another, *i. e.*, a ferromagnetic ordering of the localized spins minimizes the kinetic energy of the e_g-electrons. When the substitution degree is sufficiently high, the e_g-electrons form a ferromagnetic metallic state. As a result, in the ground state, all conducting electrons are spin-polarized in the direction of the spontaneous magnetic moment and there are no electrons with opposite spins. This type of metals is referred to as *half-metallic ferromagnet* (hmF), *i. e.*, it is a metal for the majority spin and an insulator for the minority spin [3.56].

Experimental data on manganites with a perovskite structure, where the magnetic ions are ions of a single element with different valences, are in good qualitative and quantitative agreements with this model. For example, Bowen *et al*. curried out the measurements a current's spin polarization in magnetic tunnel junctions with the manganite $La_{2/3}Sr_{1/3}MnO_3$ as the electrode material. The results obtained suggest that the electrode's current spin polarization is at least 95 % [3.57]. That is why for inducing triplet correlations in a singlet SC the high-transmission contacts of half-metallic ferromagnets and SC are most promising ones. Yet, to overcome the spin conservation low and allow for proximity induced triplet amplitudes in the ferromagnet, see Fig. 3.1, one needs an inhomogeneous non-collinear magnetization in the interface region. One such possibility is nanoparticles of hmF manganites.

Nanoparticles. A natural question arises whether the bulk characteristics of manganite are retained in nanosized samples. In Refs. [3.58–3.60] perovskite-type manganese oxide nanoparticles (NPs) with particle sizes of 15–30 nm and 100–200 nm were prepared and studied using ^{55}Mn nuclear magnetic resonance, superparamagnetic resonance, and magnetic measurements. The nuclear spin dynamics results provided direct evidence that the grain boundary of NPs is not sharp in magnetic and electrical respects, but rather should be considered as a transfer region of several (~ two) monolayers with magnetic and structural orders different from the inner part of the grain. The cores of the NPs are magnetically homogeneous. The local structure of the outer shell is that of perovskites yet modified by vacancies, stress, disordering of atoms in perovskite cells and broken bonds on the surface. The Curie temperature, determined as the magnetization onset was close to that in a bulk crystalline sample of the same composition. Electrical transport properties support this physical picture. Hence, the manganites nanoparticle's inner parts

are magnetically identical to a bulk sample of the same composition, and in the inner part the strength of the double exchange interaction and the half-metallic conductivity are preserved.

3.4 Two-dimensional Berezinskii–Kosterlitz–Thouless topological phase transition in three-dimensional nanocomposites

As already noted above, hybrid SC/hmF nano-heterostructures can enable new intelligently tailored functionality and have gained attention over the past few years as promising functional materials for superconducting spintronics. Apart the purpose of superconducting spintronics functional materials, transport properties of SC/hmF *nano*composites have been attracted a fundamental interest themselves, as well. One of the distinctive features of SC/hmF nanocomposites is an unconventional superconducting proximity effect, that determines their important characteristics to be beyond the conventional chaotic two-component nanostructures. Due to the proximity effect in SC/hmF nanocomposites, geometric contacts and electrical connectivity of individual particles are often not the same issue [3.61 - 3.65].

To date, a few works have been reported on the study of transport properties of a SC with half-metallic magnetic nanoparticles composites. Unconventional double percolation transition was identified by Liu *et al.* [3.61] for a binary network composed of MgB_2 superconductor and CrO_2 hmF nanoparticles. It was shown that the double percolation transition (superconductor–insulator–metal) is controlled by volume fractions of the components and originates from the suppressed interface conduction and tunneling as well as a large geometric disparity between particles [3.61]. In Ref. [3.62], Acharya *et al*. prepared and studied electrical transport characteristics of $Bi_2Sr_2CaCu_2O_8/BiFeO_3$ nanocomposite with various weight percentage of superparamagnetic $BiFeO_3$ nanoparticles. Measurement of the critical current density reveals that the superconducting transition temperature splits into two ones, T_{C1} and T_{C2}, along with broadening of overall superconducting transition. Such behavior has been attributed to a weak-link nature of a granular SC as the latter is composed of superconducting grains embedded in a non-superconducting host. The point is that for nanoparticles the geometric contacts and

electrical connectivity of individual particles are often not the same. Of the two superconducting transitions temperatures, the higher one, T_{C1}, marks the superconductivity in grains' balk whereas the grain boundary remains normal, and the lower one, T_{C2}, emerges when the grain boundary becomes superconducting, too.

Conventional Berezinskii–Kosterlitz–Thouless (BKT) transition [3.66–3.68] in the case of superconducting system has topological nature and is associated with a vortex-antivortex (un-) binding [3.69]. At temperatures below T_{BKT}, the vortex-antivortex pairs composite a bound state; for $T > T_{BKT}$, the vortex proliferation takes place, and the system enters a Coulomb gas-type state. This BKT topological transition is general and was observed in many two-dimensional systems, such as superfluid and superconducting films [3.70], two-dimensional spin systems [3.71, 3.72], *etc.* Although the BKT transition is a well-known phenomenon on planar surfaces, for curved spaces the situation is not so clear. The realization of a classical BKT transition in nominally three-dimensional systems has not an obvious case *a priori* [3.73, 3.74], as well.

It is well known that in the vicinity of the BKT transition to a superconducting state the resistance of thin films is described by the expression (see, *e. g.*, the review [3.69] and references therein):

$$R(T) = R_0 \exp\left\{-4\alpha\left[\frac{T_{C0} - T_{BKT}}{T - T_{BKT}}\right]^{1/2}\right\}. \qquad (3.1)$$

Here the parameter α is uniquely expressed in terms of the effective mass of the core of a fluctuating vortex and an antivortex. It was shown [3.74] that α is not an arbitrary constant of the order of unity but is causally related to the effective mass μ of the vortex core in a two-dimensional (2D) SC. To be exact, $\alpha = \mu/\mu_{XY}$ where μ_{XY} stands for the mass of the vortex core in the classical XY model. In the most cases, when the two-dimensional nature of the film's superconducting transition is not in doubt, and especially for high-T_C cuprate SCs, the ratio $\alpha = \mu/\mu_{XY}$ turned out to be limited by a rather narrow interval of $1 \lesssim \alpha \lesssim 1.5$ [3.75, 3.76].

3.4.1 s-wave superconductor

In this subsection, we discuss transition from the normal state to superconducting one in chaotic two-component nanostructures, which are nanocomposites consisting of MgB_2 superconductor microparticles and nanoparticles of a half-metallic $La_{2/3}Sr_{1/3}MnO_3$ (LSMO) ferromagnet (see Ref. [3.33]).

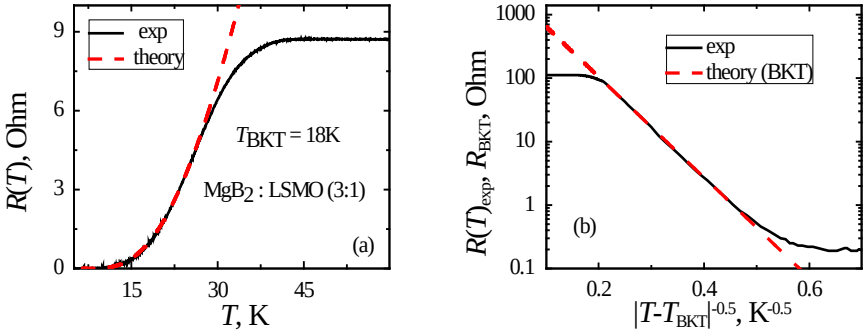

Fig. 3.2 – (a) Experimental (solid curve) and theoretical [dashed curve, Eq. (3.1)] dependences R(T) for the $MgB_2/La_{2/3}Sr_{1/3}MnO_3$ (3:1) nanocomposite. (b) The same dependences represented in a logarithmic scale on the ordinate axis. Adapted from Ref. [3.33]

Figure 3.2(a) displays typical temperature dependence of the nanocomposite resistance $R(T)$ (solid line) in a broad temperature range. In addition to a steep fall of resistance at $T < T_C$ that is typical of manganites (not shown in the plot), there is a virtually linear dependence $R(T)$ in the $T^* < T < T_C$ temperature range that is followed by a significant decrease in resistance at a temperature of $T^* \approx 40$ K $\approx T_{C0}(MgB_2) \approx 39$ K, Fig. 3.2(a). Figure 3.2(b) displays the same dependence in a logarithmic scale on the ordinate axis. The most interesting observation is that the temperature behavior of the resistance at $T < T_{C0}$ is surprisingly well described by Eq. (3.1) [dashed lines in Figs. 3.2(a) and 3.2(b)]. Thus, the $R(T)$ behavior points that in the three-dimensional (3D) nanocomposite, transition to a superconducting state goes through a BKT transition similarly to a 2D system with the transition temperature $T_{BKT} \approx 18$ K and parameter $\alpha = 1 – 1.2$. It should be noted that the theoretical Eq. (3.1) and experimental $R(T)$ dependences agree well in a broad temperature range of $T_{C0} – T_{BKT} \approx 20$ K, where the resistance varies by three orders of magnitude.

The transport characteristics of the nanocomposite also proved to be very sensitive to the external high-frequency (HF) irradiation. Figure 3.3(a) shows the effect of the HF irradiation on resistive transitions in the temperature range $T_{BKT} < T < T_{C0}$. It should be noted that the HF signal applied to the MgB_2 sample does not result in significant changes in the $R(T)$ dependence [see the $R(T)$ dependence for MgB_2 in Fig. 3.3(a)]. At the same time, the resistance of a nanocomposite increases inder the HF irradiation. The HF-signal caused changes in the current-voltage *(I–V)* characteristics of the nanocomposite are shown in Fig. 3.3(b). The increase of the resistance and the decrease of the excess current under the influence of a small amplitude of the electromagnetic signal indicate that weak couplings (Josephson-like contacts) in the $–MgB_2–$ LSMO$–MgB_2–$ chains are suppressed.

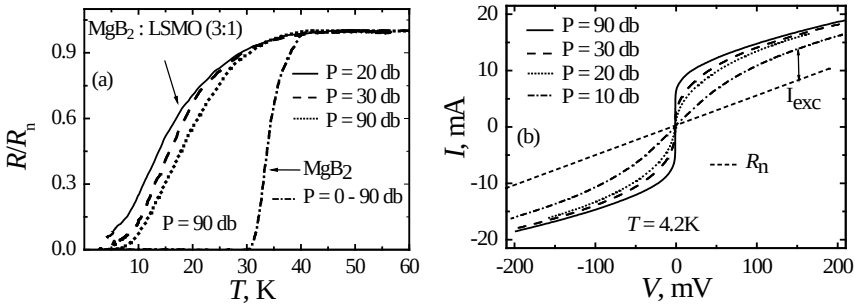

Fig. 3.3 – The effect of the HF irradiation on the (a) resistive transition and (b) current-voltage characteristics of $MgB_2/La_{2/3}Sr_{1/3}MnO_3$ (3:1) nanocomposite. The straight dashed line is plotted to visualize the effect of the HF irradiation on the excess current I_{exc} at $T = 4.2$ K. Adapted from Ref. [3.33]

According to the classical BCS theory of superconductivity, an equilibrium density of Cooper pairs at the temperature T_{C0} exists concurently with the onset of a dissipation-free state. The superconducting state of the system is described by a complex order parameter

$$\Phi(\mathbf{r}) = |\Phi| \exp\{\varphi(\mathbf{r})\}, \qquad (3.2)$$

where $|\Phi| \equiv \Delta$ is the binding energy of a Cooper pair, and the phase $\varphi(\mathbf{r})$ characterizes the coherent state of Cooper pairs. In the absence of the current in a superconductor, $\varphi(\mathbf{r})$ = const. In 3D systems, the destruction of superconductivity usually occurs via vanishing the order-parameter modulus $|\Phi|$,

due to an increase in temperature to T_{C0} or under the action of a magnetic field having a critical magnitude. Distinguishing feature of 2D superconducting systems is that a gas of fluctuations may exist in the form of spontaneously generated magnetic vortices at a temperature below the temperature T_{C0} of the bulk superconducting transition (see, for example, the review [3.69]). The vortices are generated in pairs with opposite directions of ring currents (vortex–antivortex pairs), which annihilate after a finite time because of collisions. In a zero magnetic field, the number of vortices having opposite signs is the same and is determined by the dynamic equilibrium between their spontaneous generation and annihilation. The wave-function phase changes because of going around an immobile vortex by 2π; therefore, the free motion of vortices results in fluctuations of the phase. If the amplitude of the fluctuations is large enough, the coherence of the superconducting state is lost. The order parameter modulus Δ remains non-zero in most of the sample volume (and vanishes only near the vortex axis).

If the temperature decreases, the BKT transition occurs at some temperature T_{BKT} ($< T_{C0}$): vortex pairs are no longer generated, vortex density sharply decreases to become exponentially small, and dissipation becomes exponentially small as well. Thus, in the $T_{BKT} < T < T_{C0}$ temperature range, Cooper pairs coexist in 2D superconductors with vortices. Dissipation decreases due to the presence of Cooper pairs but does not vanish. In samples with defects, the BKT transition broadens due to internal non-uniformities, and this circumstance should be considered to ensure that the numerical estimates of system parameters are correct [3.75, 3.76].

If a sample consists of superconducting granules embedded into a normal (non-magnetic) metal, the superconducting state is destroyed by another mechanism: transition to the resistive state occurring due to the loss of phase coherence in the system with a finite order parameter modulus $|\Phi|$ in individual superconducting granules (see, for example, the review [3.77]). This implies that the system is in the dissipative state, while individual granules remain in the superconducting state. In this case, charge may be transferred from one granule to another via two channels $j_{tot} = j_S + j_N$: by the Josephson current j_S and uncorrelated electrons j_N. If charge is transferred by the Josephson current of Cooper pairs, the phases of the order parameter between granules partici-

pating in the current transfer are correlated, and a macroscopic superconducting state is established between them. However, the Josephson currents can be suppressed by fluctuations, such as due to a large normal resistivity between granules or external influences. Then the charge is transferred between the granules due to single-particle excitations, $j_{tot} \rightarrow j_N = eN_e$, the concentration of which, N_e, is exponentially small in the granules due to their superconducting state: $N_e \propto \exp(-\Delta/T)$ (e is the electron charge). In the general case, a resistive state with a non-zero equilibrium density of Cooper pairs is realized in the system. This is manifested experimentally by the emergence of an excess current in the current-voltage characteristics of the sample.

Specific features of the BKT transitions in superconductor / normal metal (SC/N) proximity structures were studied in Refs. [3.78–3.80]. Particularly, in proximity Pb–Sn film contacts in the temperature range $T_{C0}(\text{Sn}) \approx 3.75$ K < $T < T_{C0}(\text{Pb}) \approx 7.3$ K the authors of Ref. [3.78] observed a resistive transition to the superconducting state that reproduces the main features of the BKT transition. In the same temperature range, nonlinear current-voltage characteristics were observed as it had been predicted in Ref. [3.79] for the case of the topological ordering of vortices in 2D superconductors.

Although the layered proximity SC/hmF structures have been actively studied using both experimentally and theoretically (see, for example, reviews [3.26, 3.45, 3.51] and references therein), a satisfactory description of the properties of SC/hmF nanocomposite materials is still missing. As was noted above, main characteristics of SC/hmF nanocomposites (critical transition temperatures, current-voltage characteristics, percolation transition thresholds, etc.), most likely, cannot be quantitatively described by standard percolation models (see a discussion in Refs. [3.33, 3.34]). The analysis of the structure of the MgB_2/LSMO nanocomposite shows that nanosized LSMO grains fully ‘cover’ the significantly larger MgB_2 granules. This assumption is supported by measurements of sample density after pressing. For example, the density of the MgB_2 plates produced under a pressure of 40–60 kbar is (72 ± 3) % of the MgB_2 single crystal density. The density of the LSMO nanopowder compressed under the same pressure was a mere (68 ± 3) % of the single-crystal density. At the same time, the density of the MgB_2/LSMO (26 % LSMO) composite was (96 ± 3) % of the calculated value. Such a high

composite density indicates that the LSMO nanoparticles ‘spread’ under high uniaxial pressure across the sample volume, filling in pores that surround large MgB_2 granules.

Under these types of conditions, the onset of superconductivity occurs in each MgB_2 microgranule independently, and BCS-type fluctuations are formed at the temperature of the condensate formation in bulk MgB_2. The magnetic fluxes caused by the magnetization of manganite nanoparticles are coupled to these nanoparticles and no longer fluctuate at temperatures $T << T_C$. A resistive state emerges in the nanocomposite, featuring a nonzero equilibrium concentration of Cooper pairs and a frozen magnetic field created by the LSMO nanoparticles. If the temperature decreases further, a (quasi-) two-dimensional structure is most likely formed in the system in the $T_{BKT} < T < T_{c0}$ temperature range; it consists of superconducting granules covered by ferromagnetic nanoparticles (hmF–SC–hmF). The manganite nanoparticles contacting with MgB_2 transitioned to the superconducting (triplet) state induced by the proximity effect [3.28–3.30].

This physical model provides an explanation for the agreement between the observed dependence $R(T)$ (Fig. 3.2) and Eq. (3.1) deduced for 2D systems. Thus, we are dealing with a composite, the main resistive losses of which are caused by current flowing through the ferromagnetic LSMO granules that cover the MgB_2 granules (an analog of a 2D shell / plane). As the temperature decreases, the processes that result in the BKT transition are realized in the two-dimensional superconducting LSMO layers (contacting with MgB_2). In the superconducting state of the nanocomposite, an overcurrent flows through the Josephson-like junctions –SC–hmF–SC–hmF–SC–. If the nanocomposite is irradiated with a small-amplitude HF signal, the currents induced by the HF signal are sufficient to suppress weak Josephson junctions between superconducting LSMO nanoparticles. This contributes to the creation of single-particle charge carriers, which is recorded as the emergence of additional resistance and the decrease in the excess current (Fig. 3.3). That is, in the nanocomposite, the main effect of the high frequency field is the destruction of the coherent state of weakly linked Josephson junctions formed by manganite layers that are in a superconducting state due to the proximity effect (for more details, see Ref. [3.81, 3.82]).

3.4.2 d-wave superconductor

MgB_2 is an *s*-wave superconductor. In this subsection, we discuss results of experimental investigations and theoretical analysis of the transition to a superconducting state of random binary nanocomposites of *d*-wave cuprate SC $Bi_2Sr_2Ca_2Cu_3O_{6+x}$ (Bi2223) microparticles and hmF $La_{2/3}Sr_{1/3}MnO_3$ (LSMO) nanoparticles – Bi2223/LSMO nanocomposites [3.34, 3.35].

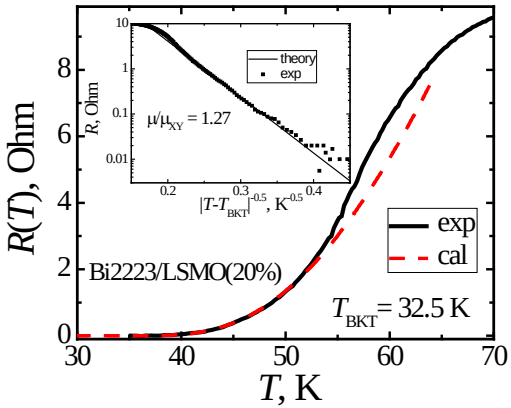

Fig. 3.4 – The nanocomposite's (20 % LSMO) resistance temperature dependence. *Main panel:* Experimental, black solid curve, and theoretical, Eq. (3.1), red dashed curve, $R(T)$ behavior. *Insert*: Effective $\alpha = \mu/\mu_{XY}$ where μ_{XY} is the vortex core mass in the classical XY model. Adapted from Ref. [3.35]

Figure 3.4 displays experimental temperature dependence of the 20 vol. % of LSMO nanocomposite (black solid line) resistance $R(T)$ in a temperature range below T_{C0} of Bi2223. In addition to a steep fall of resistance at $T < T_{C0}$, there is a virtually parabolic dependence $R(T)$ in the temperature range ~ 30–60 K that is followed by a significant decrease in resistance. The most interesting observation is that the nanocomposite's resistance temperature behavior at $T < 55$ K is surprisingly well described by Eq. (3.1), red dashed curve in Fig. 3.4. It should be noted that the theoretical Eq. (3.1) and experimental $R(T)$ dependences agree well in a broad temperature range of $\Delta T \approx 32 \div 55$ K, where the resistance R varies by three orders of magnitude. Such $R(T)$ dependence points that the 3D nanocomposite goes through the BKT-like transition similarly to a 2D system with the transition temperature $T_{BKT} \approx 32.5$ K and the parameter α equals to ≈ 1.27.

In the context of the genuine BKT transition broadening in inhomogeneous layered SCs, the temperature behavior of the *I–V* characteristic should correspond to the dependence $V \sim |I|^{a(T)}$, with the exponent $a(T_{BKT}) = 3$ and $a(T) \to 1$ above T_{BKT} [3.75, 3.76, 3.79, 3.80]. Figure 3.5 (a) displays a logarithmic plot of *I–V* characteristics of the sample with 20 % LSMO at temperatures spanning the range $T_{BKT} \leq T < T_{C0}$. At $T = 52.5$ K the *I–V* curve is approximately linear, while at T_{BKT}, $V \sim I^3$. Experimental (points) temperature dependence of the parameter $a(T)$ in $V \sim |I|^{a(T)}$ dependence is shown in Fig. 3.5 (b), as well. The choice of T_{BKT} which provides the best fit to the resistance theory [3.79, 3.80] also corresponds to the value at which the *I–V* curves have an exponent $a(T_{BKT}) \approx 3$. Again, we have observed that the transition to a superconducting state, the 3D nanocomposite's *I–V* characteristics, are well described within a 2D topological transition approach and is associated with the BKT-like superconducting transition [3.75, 3.76, 3.79, 3.80].

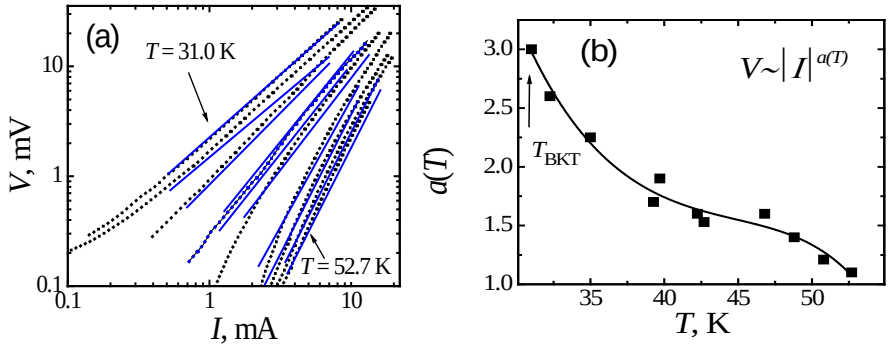

Fig. 3.5 – (a) Logarithmic plot of *I–V* characteristics of the sample 20 % LSMO at temperatures spanning the range $T_{BKT} \leq T < T_{C0}$ (T = 31.0 K, 32.3 K, 39.3 K, 39.7 K, 42.3 K, 42.7 K, 46.8 K, 48.8 K, 50.8 K, 52.7 K); points – experiment, blue solid lines – theory. (b) Experimental data (points) and quadratic approximation (solid line) for the temperature dependence of the parameter $a(T)$, $V \sim |I|^{a(T)}$. Adapted from Ref. [3.35]

As in the case of the MgB_2/LSMO nanocomposite, it is naturally to suggest that the Bs2223/LSMO sample's resistivity distinctive features are determined by an inhomogeneous spatial distribution of the local superconducting grains coupled by Josephson currents. The validity of the experimental data interpretation has been supported by the effect of an external HF radiation on the nanocomposite's transport characteristics.

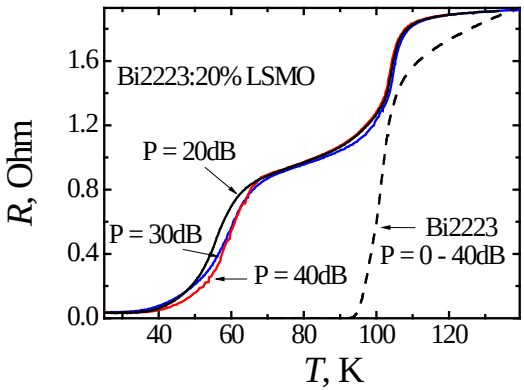

Fig. 3.6 – Effect of the HF radiation ~ 100 MHz on the resistive transition of a Bi2223 sample and nanocomposites with 20 % of LSMO. Adapted from Ref. [3.35]

Figure 3.6 demonstrates the effect of the HF irradiation on resistive transitions in the temperature range $T < T_{C0}$ in the nanocomposites Bi2223/20%LSMO and in compacted Bi2223 sample. As it is shown in Fig. 3.6, the HF signal applied to the compacted Bi2223 sample does not cause noticeable changes in the $R(T)$ dependence. At the same time, when the nanocomposite is a subject of the HF irradiation, a tail with an upward curvature change demonstrating increasing resistance. This is typical for the fluctuation resistivity near the T_{BKT} transition [3.77] when the resistive tail can be attributed to the inhomogeneous spatial distribution of the local superfluid, caused by intrinsic inhomogeneous density distribution in the systems.

The changes in the I-V characteristics of the 20 % LSMO nanocomposite's superconducting state under the HF radiation are shown in Fig. 3.7. At small amplitudes of the electromagnetic signal, an increase in the resistance and a decrease in the excess current indicates that weak couplings (Josephson-like contacts) are suppressed in the –Bi2223–LSMO–Bi2223– chains. Thus, the transport characteristics of the 3D nanocomposite are extremely sensitive to the external HF radiation.

Thus, as for the MgB_2/LSMO nanocomposite, in the case of the Bi2223/LSMO nanocomposite the proximity effect possesses a few specific peculiarities.

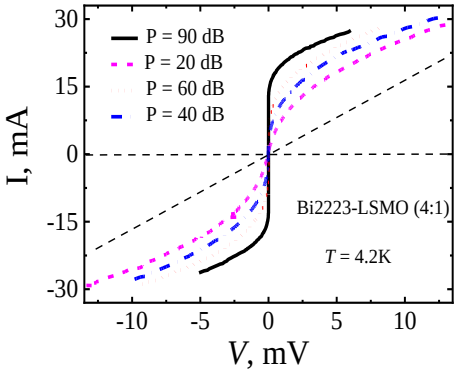

Fig. 3.7 – Effect of the HF radiation ~ 100 MHz on current-voltage characteristics of the nanocomposite with 20 % LSMO. Adapted from Ref. [3.35]

First, because the contacts between Bi2223 grains are in the bulk through the half-metallic LSMO *nano*grains, this causes significant broadening of the nanocomposite transition to a superconducting state. Second, for high-T_C SCs with a *d*-wave Cooper pair symmetry [3.26], theory predicts, and experiment provides evidence that in proximity coupled *d*-wave SC/ferromagnet structures an unconventional (spin-triplet) superconducting state can be generated. This also means that in the nanocomposite a new geometrical length has been generated that characterizes unconventional superconducting state (a mixture of *d*-wave singlet and *p*-wave triplet Cooper pairs) in the proximity-coupled regions.

3.4.3 Discussion

The main physical message of the experimental data shown in Figs. 3.2–3.7 is that the observed Berezinskii–Kosterlitz–Thouless-like behavior of the transport properties of nanocomposites are due to two scales typical for this type of systems. Namely, they are (i) a significant difference between the geometric dimensions of the components and (ii) a *p*-wave superconducting state of the LSMO nanoparticles induced by the proximity effect.

In bulk (three-dimensional, 3D) composite systems superconductivity has been studied within the percolation scenario. It is well established, when the grains of a superconducting material, *d*, are large enough, $d >> \xi_S$, their basic

intra-granular characteristics (critical temperature, superconducting gap, etc.) are not affected by the proximity of the non-superconducting component and remain close to the bulk value of a quantity both above and below a percolation threshold. For a bulk composite with roughly the *same geometrical size* of components, the lattice percolation model [3.83–3.85] predicts $f_C = 0.16 \pm 0.02$ for the percolation threshold of the volume fraction, f, of a superconducting component (f_C being a percolation threshold of superconducting grains with the linear dimensions $\gtrsim \xi_S$). Thus, according to the conventional lattice percolation model, for the nanocomposite systems under consideration with large grains of the superconducting material, above the percolation threshold of the volume fraction f_C, the macroscopic transition temperature T_C should not be strongly dependent on the contents variation. However, even for the SC/hmF samples with the volume fraction $f \sim 0.6$, *i. e.*, about three times larger than the conventional percolation model predicts, there is no transition into a superconducting state. Moreover, as it follows for the $R(T)$ data [3.33, 3.35] the transition temperature T_C is strongly reduced for the samples with 80, 75, and 70 vol. % of the superconducting component (20, 25, and 30 vol. % of LSMO), *i. e.*, even at concentrations when an infinite percolating cluster of MgB_2 or Bi2223 grains should be formed. Thus, the predictions based on the conventional percolation models fail for the *s-(d-)*-wave SC/hmF nanocomposites most probably due to two factors: (i) essential difference in the components' geometrical size and (ii) unconventional (spin-triplet) superconducting proximity effect.

As is known, below the superconducting transition, an indirect (due to the proximity effect) coupling between constituent components emerges. In SC/hmF heterostructures a long-range proximity effect will be realized effectively, and a triplet component of anomalous correlations should be taken into consideration if there is a spatial variation of the magnetization at the ferromagnet surface [3.23–3.26, 3.37–3.43, 3.86–3.90]. Characteristic coherence length of triplet correlations $\xi_F = (D_F/2\pi T)^{1/2}$ can be as large as ~ 100 nm at low temperatures. In previous works, anomalous superconductivity has been indeed detected in SC/hmF nanostructures [3.30, 3.38] and in SC/hmF junctions [3.23, 3.25, 3.28, 3.39]. It was argued that at low temperatures, manganites are thermodynamically close to a superconducting state with a triplet

p-wave even frequency pairing [3.28–3.30, 3.36]. Being proximity coupled to a singlet SC, the $m = 0$ triplet wave-function component is coupled in the manganite via the boundary condition to the singlet pairing amplitude in the SC counterpart. At the same time, the spin-active boundary leads to coupling of the $m = 0$ triplet component with an equal-spin, $m = 1$, pairing amplitude in the manganite. These couplings yield phase coherency of both $m = 0$ and equal-spin $m = 1$ triplet Cooper pairs in the hmF manganite. Dependence of the scale of superconducting correlations on the intrinsic magnetic field inhomogeneity is a feature of the proximity effect in mesoscopic hmF/SC structures [3.26, 3.43, 3.44, 3.51, 3.86 - 3.90].

Under these specific conditions, the nanocomposite's transition to a superconducting state, most probably, is followed the next 'evolution scenario'. The onset of superconductivity occurs independently in each SC microgranules at the temperature of superconducting condensate formation in the bulk SC. Magnetic fluxes are caused by the manganite nanoparticles' magnetization and at temperatures $T < T_{C0} < T_{Curie}$ (LSMO) magnetic fluxes are confined to the manganite nanoparticles. That is, in the temperature range $T_{BKT} < T < T_{C0}$, a resistive state emerged in the nanocomposite is featured by a nonzero equilibrium concentration of Cooper pairs in the SC microparticles and frozen magnetic vortices created by the LSMO nanoparticles. A 3D structure is formed in the system. It consists of the superconducting granules covered by the ferromagnetic nanoparticles: –hmF–SC–hmF–SC– 'brickwork' structure. If the temperature decreases further, BKT-like superconducting correlations in the bulk *s*-(*d*-)-wave SC/LSMO nanocomposite emerge due to the emergence of the effective 2D percolation cluster of a specific superconducting state. Namely, the 2D supercurrent percolation is fulfilled through hmF nanoparticles layer following the 'brickwork' scheme. Due to the proximity effect at magnetically inhomogeneous SC-LSMO interfaces, the superconducting state of the percolation layer is a mixture of *s-(d-)*-wave singlet and *p*-wave triplet Cooper pairs.

3.5 Triple-gap superconductivity of MgB_2–(La, Sr)MnO_3 nanocomposite

Another topic of nowadays fundamental interest is a spatial inhomogeneity in the superconducting density of states and the superconducting state, which is governed by quantum phase fluctuations [3.91–3.95]. Most mean-field theories assume that the relation $T_\phi > T_\Delta$ is fulfilled between the temperatures of electron pairing T_Δ and the long-range phase coherency T_ϕ. This means that global phase coherency and the energy gap appear (vanish) at the same temperature, mainly due to the opening (disappearing) of the gap with temperature. However, it has been shown (see, *e. g.*, reviews [3.77, 3.91]) that for systems with low conductivity and small superfluid density (bad metals), the temperature of the global phase coherency T_ϕ is reduced significantly and becomes to be comparable to or even smaller than the pairing temperature T_Δ. In this case, the critical temperature T_C is determined by the global phase coherency, whereas a local pair condensate could exist well above T_C. For high-T_C cuprates diamagnetism due to fluctuating superconducting pairs above the superconducting transition temperature as well as the origin of the so-called pseudogap still remain under discussion (see, *e. g.,* Refs. [3.92–3.95] and references therein). A new stimulus for active debates in this area is motivated by the search for materials with triplet fluctuation superconductivity.

At energies below the superconducting gap, the charge transport through a normal nonmagnetic (N) metal in contact with a SC is possible only due to a specific process called Andreev reflection (AR) [3.49, 3.96–3.98]. This is a two-particle process in which, in the N metal, an incident electron above the Fermi energy E_F and an electron below E_F with the opposite spin are coupled together and transferred across the interface into the SC side, forming a Cooper pair in the condensate. Simultaneously, an evanescent hole with opposite momentum and spin emerges in the N metal. The charge doubling at the interface enhances the sub-gap conductance and this phenomenon has indeed been observed in the case of a perfectly transparent interface. The picture is significantly modified when spin comes into play. If the N metal is a half-metallic ferromagnet, there is full imbalance between spin-up and spin-down populations, which suppresses the AR and reduces the sub-gap conductance to zero.

According to the existing publications [3.99–3.102] the charge carrier polarization for LCMO is large, greater than 75 %. Thus, if a supercurrent in

the composite is unpolarized [an *s*-wave or a *p*-wave ($S = 1$, $m = 0$) component of triplet pairing] the AR will be suppressed, and the sub-gap conductance will be reduced below the normal-state value. On the contrary, if at both sides of the contact the charge current is spin polarized, there is no restriction (because of spin) on the AR and, as in the conventional case [3.96–3.98] an excess current and a doubling of the normal-state conductance are observed.

Figure 3.8 shows representative dynamic conductance spectra $dI/dV = G(V)$ of micro-constrictions between In, Ag, and Nb tips and the sample 3:1 (a configuration commonly called the 'needle anvil') measured at $T = 4.2$ K. At low voltages, conductance peaks corresponding to *three* superconducting gaps with energies $\Delta(\pi) = 2.0 – 2.4$ meV, $\Delta(\sigma) = 8.4 – 11.7$ meV, and $\Delta_{tr} = 19.8 – 22.4$ meV are clearly observed. (In the figure, the position of the dI/dV minimum is denoted by Δ. For PCs with not too large lifetime-broadening effects, this value does not differ much from the proper energy gap [3.103]). Two of the gaps, $\Delta(\pi)$ and $\Delta(\sigma)$, were identified as MgB_2 gaps (to be precise, as ones originating from the $\Delta(\pi)$ and $\Delta(\sigma)$ gaps of MgB_2, respectively). The magnitude of the smallest $\Delta(\pi)$ gap remains in the range of the bulk MgB_2 gap [3.104]; the gap $\Delta(\sigma)$ was recognized as *enhanced* MgB_2 $\Delta(\sigma)$ gap.

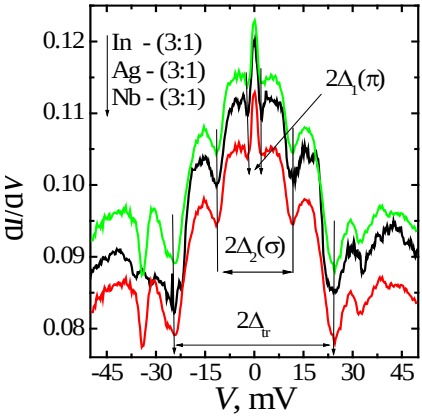

Fig. 3.8 – Point-contact Andreev reflection spectra of In, Ag, and Nb tips and $MgB_2/La_{0.67}Sr_{0.33}MnO_3$ (3:1) nanocomposite; $T = 4.2$K. Adapted from Ref. [3.30]

The third gap, Δ_{tr}, the authors [3.30] attributed to the intrinsic superconducting pairing in the (La, Sr)MnO_3 compound. The absolute value of Δ_{tr} is the same as those also detected in PCs of (La, Sr)MnO_3 and (La,Ca)MnO_3

with Pb or MgB_2 [3.28, 3.29, 3.102]. The magnitude of Δ_{tr} is more than *three times larger* than the largest 'parents' $\Delta(\sigma)$ = 6.8–7.1 meV MgB_2 gap [3.104]. Note that the PCs' resistivity varied by orders of magnitude, while the multiple-gap structure in the quasiparticle density of states, as well as the gap energy values, were robust features and reproduced in all PCs have been prepared.

In Fig. 3.9, we present an experimental temperature dependence of the energy gap $\Delta_{tr}(T)$ [3.30]. For comparison, the conventional Bardeen–Cooper–Schrieffer BCS gap temperature behavior is shown in the figure, too. From the BCS relation $\Delta(0) = 1.76k_BT_C$, the $\Delta_{tr}(0)$ = 19.8–22.4 meV gap would lead to a superconducting state with $T_C \approx 120$ K. Yet, the energy gap $\Delta_{tr}(T)$ vanishes as the temperature increases towards $T_C \approx 39$ K of MgB_2. Evidently, the experimental behavior of $\Delta_{tr}(T)$ does not follow the BCS dependence. The temperature dependence of the largest gap detected, $\Delta_{tr}(T)$, directly proves that its emergence is not an 'independent' property but is due to the superconducting state of MgB_2, *i. e.*, due to the proximity effect.

The results presented in Figs. 3.8 and 3.9 convincingly show that, at low temperatures, a noncoherent *p*-wave even-frequency spin-triplet superconducting condensate already exists in half-metallic manganites. Being proximity coupled to the singlet SC, the $m = 0$ triplet component in the manganite is coupled via the boundary condition to the singlet pairing amplitude in the SC partner.

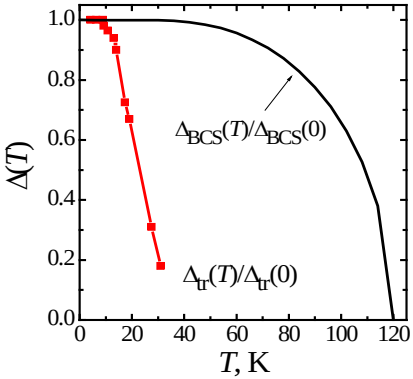

Fig. 3.9 – Experimental (square points) $\Delta_{tr}(T)$ gap temperature behavior (normalized to the zero-temperature gap) of the $MgB_2/La_{0.67}Sr_{0.33}MnO_3$ (3:1) nanocomposite and the BCS gap temperature dependence (black solid line). Adapted from Ref. [3.30]

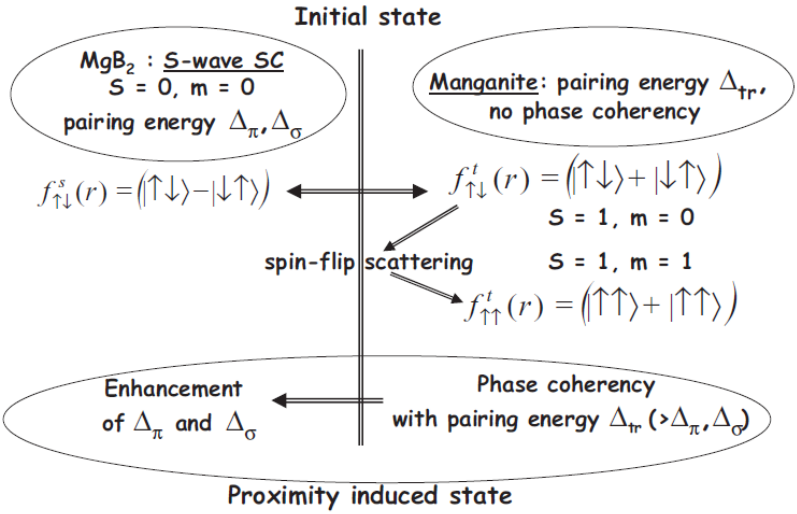

Fig. 3.10 – A sketch of the long-range phase coherency due to the proximity effect in the SC/hmF nanostructures. Adapted from Ref. [3.30]

At the same time, the spin-active boundary leads to coupling of the $m = 0$ triplet component with an equal-spin, $m = 1$, pairing amplitude in manganite. These couplings yield phase coherency of both $m = 0$ and equal-spin $m = 1$ triplet Cooper pairs in the HMF with a large quasiparticle gap Δ_{tr} ($> \Delta_\pi, \Delta_\sigma$). As an inverse effect, being proximity linked to the *s*-wave pairing amplitude, the $m = 0$ amplitude of the triplet superconducting state enhances the quasiparticle gap(s) of a singlet SC. Fig. 3.10 illustrates the described mechanism of the long-range phase coherency due to the proximity effect in the nanocomposite.

3.6 Local triplet superconductivity of half-metallic manganites

As was noted above, the transition to the superconducting state is accompanied and is caused by a rearrangement of the electronic spectrum with the appearance of a gap at the Fermi level. The state is characterized by a complex order parameter (see, *e. g.*, reviews [3.77, 3.91]):

$$\Delta(\mathbf{r}) = |\Delta(\mathbf{r})|\exp\{i\varphi(\mathbf{r})\}, \qquad (3.3)$$

where the modulus of the pairing energy, namely $2|\Delta(\mathbf{r})|$, is the gap value in the electronic spectrum. In the mean field theory, temperatures of the electron-pairing effect, T_Δ, and the long-range (global) phase coherency, T_φ, coincide and yield the critical temperature, T_C. This implies that the spatial variations in $|\Delta(\mathbf{r})|$ are small, and that global phase coherence temperature T_φ is larger than (or equal to) T_C.

In a system with a small superfluid density (bad metals with an electron concentration that is substantially less than that characteristic of conventional metals) the spatial variations / fluctuations in the order parameter $\Delta(\mathbf{r})$, *e. g.*, due to thermal effects, become crucial in the regions where pairing energy value $|\Delta(\mathbf{r})|$ is small. As the result, in a bad metal, thermal fluctuations in the global phase coherency of the order parameter are the most important ones. The fluctuations of the order parameter phase $\varphi(\mathbf{r})$ in mesoscopic 'islands' prevent the long-range superconductivity. Therefore, for systems with low conductivity and small superfluid density, the temperature of the system's global phase coherency T_φ can be reduced significantly and could be smaller than the 'islands' pairing temperature T_Δ. Then the superconducting transition temperature T_C is determined by the global phase coherency, whereas the pair condensate could exist well above $T_C = T_\varphi < T_\Delta$ [3.77, 3.91–3.95].

An important consequence of Cooper pairs fluctuation above the transition temperature T_C is the appearance of the so-called pseudo-gap [3.77, 3.92–3.95], *i. e.*, a reduction of the single-electron density of states near the Fermi level. According to the viewpoint expressed in Ref. [3.92], the pseudo-gap state in high-T_C cuprates could be considered as an unconventional metal, i. e., as a SC which has lost its phase stiffness due to phase fluctuations. Doped manganites belong to bad metals, and a large pseudo-gap is detected in numerous experiments on manganites [3.105–3.108]. It may be suggested that at least a part of the observed pseudo-gap value is due to pairing without the global phase coherency. In cuprates, an additional argument for the local pair's condensate existence at $T > T_C$ is a diamagnetism observed just above T_C, i. e., when temperature $T_\varphi < T < T_\Delta$ (see, *e. g.*, Refs. [3.109, 3.110]). For manganites, however, this kind of the superfluid density precursor can be strongly suppressed by a ferromagnetic order of the localized moments and a spin-triplet state of the pair condensate.

As noted above, materials realizing spin-triplet *p*-wave pairing are a subject of special interest. This interest is motivated as systems where specific topologically protected quasiparticle excitations can be realized and as promising materials yielding novel technological applications. Long-range proximity effects interpreted in terms of singlet-to-triplet pairing conversion have been found in various SC/F systems [3.40, 3.41, 3.43, 3.51]. Among these systems, the half-metallic-based SC/F heterostructures, where long-range proximity effect has been experimentally observed, have attracted especial attention [3.24–3.26, 3.51]. As was shown theoretically, for the SC/F systems, long-range proximity effect and singlet-to-triplet pairing conversion can be realized due to interfacial magnetic inhomogeneities. Eschrig *et al.* showed that when normal metal is half-metallic ferromagnet, even frequency pairing would be mostly of the *p*-wave symmetry [3.111].

These results are compelling arguments that proximity induced superconducting transition in doped manganites follows the scenario of a 'latent' high-T_C superconductivity in doped manganites. At low temperatures, incoherent superconducting fluctuations are essentially sustained in half-metallic manganites. Although the local gap amplitude is large, there is no phase stiffness, and the system is incapable of displaying a long-range superconducting response. Nonetheless, a local phase rigidity (a local triplet pairing condensate) survives, and, in a proximity-affected region, the singlet SC establishes phase coherence of the *p*-wave spin-triplet superconducting state of the manganites [3.28–3.30].

3.7 Bosonic scenario of a local triplet superconductivity of half-metallic manganites

Let us make some suggestions concerning the mechanism of coupling spin-polarized conducting electrons in manganites and the origin of the quasiparticle gap Δ_{tr} whose magnitude cannot be explained in terms of the conventional proximity-effect theory.

In the context of manganite's half-metallic conductivity in the ferromagnetic state, a natural question arises about triplet superconductivity due to magnon coupling. The replacement of a phonon by a spin wave should not

lead to a drastic modification of superconducting properties. However, there is an important difference between these couplings [3.112]. Namely, a spin-wave excitation (magnon) carries a spin with the projection opposite to the ferromagnet magnetization direction and in the nonrelativistic approach, the projection of the total spin of both conducting and localized electrons is preserved. This means that if the magnon exchange results in equal-spin triplet pair states $\Delta_\uparrow$ or $\Delta_\downarrow$, neither $\Delta_\uparrow$ state, nor $\Delta_\downarrow$ one can exist without each other since the magnon carries spin $|S| = 1$ and thus the attraction of two electrons with the *same* spins, +1/2 (or –1/2) due to spin-wave exchange is forbidden by the spin conservation law. As Bulaevskii *et al.* showed [3.112], the spin-wave exchange mechanism leads to equal spin-triplet pairing but the resulting superconducting state is described by the two-component order parameter, $f^{tr}(\boldsymbol{r}) = g_1(\boldsymbol{r})|\uparrow\uparrow> + g_2(\boldsymbol{r})|\downarrow\downarrow>$, and *excludes a singlet* $m = 0$ pairing, $f^{tr}{}_{\uparrow\downarrow}(\boldsymbol{r}) = g_0(\boldsymbol{r})(|\uparrow\downarrow> + |\downarrow\uparrow>)$.

The conclusion that the magnon exchange excludes a singlet pairing is important in the context of the experimental results [3.28–3.31]. Broken a spin-rotation symmetry at *s*-wave SC – half-metallic manganites interface leads to spin-flip processes at the interfaces. Its origin depends on the microscopic magnetic state at the interface, the character of local magnetic moments coupling with itinerant electrons, etc. (see, e. g., [3.26, 3.51] and references therein). Due to spin mixing at the interfaces, a spin triplet ($S = 1$, $m = 0$) amplitude $f^{tr}{}_{\uparrow\downarrow}(\boldsymbol{r}) = g_0(\boldsymbol{r})(|\uparrow\downarrow> + |\downarrow\uparrow>)$ is induced by the singlet component in the *s*-wave SC, $f^{s}{}_{\uparrow\downarrow}(\boldsymbol{r}) = g_s(\boldsymbol{r})(|\uparrow\downarrow - |\downarrow\uparrow)$, and extends from the interface for about the magnetic length $\xi_F = (D_F/2\pi H_{exc})^{1/2}$ into the manganites layer. At the same time, triplet pairing correlations with equal spin pairs: $f^{tr}{}_{\uparrow\uparrow}(\boldsymbol{r}) = g_1(\boldsymbol{r})|\uparrow\uparrow>$, $m = +1$ or $f^{tr}{}_{\downarrow\downarrow}(r) = g_2(\boldsymbol{r})|\downarrow\downarrow>$ $m = -1$, are also induced (due to spin-flip processes) in the half-metallic layer. These components decay on a 'conventional' length scale $\xi_T = (D_F/2\pi T)^{1/2}$ which is much larger than ξ_F because in typical cases the exchange field H_{exc} is much larger than T_C. It is worthy to emphasis that only the $m = 0$ triplet component $f^{tr}{}_{\uparrow\downarrow}(\boldsymbol{r}) = g_0(\boldsymbol{r})(|\uparrow\downarrow> + |\downarrow\uparrow>)$ is coupled via the spin-active boundary condition to the equal-spin $m = 1$ pairing amplitudes in the half-metal. The singlet component in the *s*-wave superconductor, $f^{s}{}_{\uparrow\downarrow}(\boldsymbol{r}) = g_s(\boldsymbol{r})(|\uparrow\downarrow - |\downarrow\uparrow)$, being invariant under rotations around any quantization axis, cannot directly involved in the creation of triplet $m = \pm 1$ pairing

amplitudes in the half-metal. Taking this into account, the observed *enhancement* of MgB_2 *even-frequency singlet* Cooper pair coupling energy $\Delta(\sigma)$ means that in the manganite the $m = 0$ *even-frequency triplet* component exists, *i. e.*, the proximity induced superconducting state is described by the two-component order parameter, $f^{tr}(\boldsymbol{r}) = g_1(\boldsymbol{r})|\uparrow\uparrow> + g_2(\boldsymbol{r})(|\uparrow\downarrow> + |\downarrow\uparrow>)$. The $m = 0$ triplet component $f^{tr}{}_{\uparrow\downarrow}(\boldsymbol{r})$ is coupled via the boundary condition to the singlet pairing amplitude in the SC partner and, in this case, we deal with the 'mutual' proximity effect. As well, this points out that the most realistic coupling mechanism of the *p*-wave triplet superconductivity in half-metallic manganites is that caused by the *phonon* exchange.

As already mentioned, one of the Cooper pairs fluctuation fingerprints is the so-called pseudogap [3.77, 3.91–3.95], the reduction of the single-electron density of state near the Fermi level. At the Fermi level vicinity of manganites, a large pseudogap is observed [3.105, 3.109, 3.113, 3.114]. This experimental fact supports the hypothesis that a noncoherent *p*-wave even-frequency spin-triplet superconducting condensate already exists in half-metallic manganites at low temperatures [3.28–3.31]. Being proximity coupled to a singlet SC, the $m = 0$ triplet component in the manganite is coupled via the boundary condition to the singlet pairing amplitude in the SC counterpart. At the same time, the spin-active boundary leads to coupling of the $m = 0$ triplet component with an equal-spin, $m = 1$, pairing amplitude in manganite. These couplings yield to a phase coherency of both the $m = 0$ and equal-spin $m = 1$ triplet Cooper pairs with a large quasiparticle gap $\Delta_{tr} > \Delta(\pi), \Delta(\sigma)$. As an inverse effect, being proximity linked to the *s*-wave pairing amplitude, the $m = 0$ amplitude of the triplet superconducting state enhances the quasiparticle gap(s) in a singlet SC. Figure 3.10 illustrates the described mechanism of the long-range phase coherency due to the proximity effect in half-metallic manganites.

3.8 Half-metallic manganites – a perspective platform for high-temperature triplet superconductivity

At the actual stage of the search for topological quasiparticles in condensed matter, it is crucially desirable to identify (i) easy-to-fabricate systems possessing topological states and (ii) a way by which topologically protected

excitations can be distinguished from spurious effects. Specifically, the realization of a topological superconducting phase and Majorana quasiparticles is of the grand interest because of their novelty as well as possible applications in quantum devices. Thereupon, a convincing proof and undoubted detection of Majorana quasiparticles is among the main challenges in the general trend.

There is a variety of proposals for transforming a conventional *s*-wave SC into topological states supporting Majorana fermion excitations. For instance, realizations of Majorana bound states are expected in semiconducting-superconducting hybrid nanostructures, where the interplay between intrinsic spin-orbit coupling, proximity induced superconductivity, and external magnetic field leads to the formation of zero-energy bound states [3.17–3.21, 3.115–3.119]. An isolated zero-energy topological bound state appears in a spinless *p*-wave SC at the transition between strong- and weak-pairing phases. It is expected [3.119–3.123] that one or more Majorana bound states can appear at the opposite ends of a quantum nanoparticle wire proximity coupled to an *s*-wave SC in the presence of an applied Zeeman field. Yet, while the time-reversal symmetry can be readily broken by a magnetic field, a spin-orbit coupling is too weak to effectively break the spin-rotation symmetry and to drive the system into topologically nontrivial phase by this Kitaev scenario [3.124].

In Ref. [3.17] Choy *et. al.* proposed an alternative to Kitaev route to Majorana fermions in *s*-wave SCs that does not at all require materials with spin-orbit coupling and external Zeeman field. The authors considered a system formed by magnetic nanoparticles on a superconducting substrate. The magnetic moments are frozen, without any dynamics of their own. The nanoparticles magnetic moment breaks time-reversal symmetry as well as spin-rotation symmetry, without the need for spin-orbit coupling in the SC. The superconducting substrate induces a pairing energy in the nanoparticles, so that the system's single-band Hamiltonian has the same form as Kitaev spinless *p*-wave superconducting chain. The difference is that here the *p*-wave pairing is obtained from *s*-wave pairing due to the coupling of the electron spin to local magnetic moments (the proximity effect). In the nanoparticles wire, the transition into the topologically nontrivial superconducting phase is governed by the competition of two types of disorder: (i) variation in the

orientation of the magnetic moments on nearby nanoparticles and (ii) disorder in the hopping energies that localizes the states. The zero-energy bound states in the proximity induced *p*-wave superconducting gap, having a nonzero magnetic moment, should behave as Majorana bound states [3.17].

In the context of Ref. [3.17] conclusions, we can suggest that nanostructures based on the *s*-wave SC substrate and hmF manganites nanoparticles are the most promising and accessible systems in which Majorana fermions can be generated. Indeed, all prerequisites listed in Ref. [3.17] can be realized in the heterostructures where magnetic nanoparticles are $(La_{1-x}R_x)MnO_3$, R = Ca, Sr, … ones. Due to the ferromagnetic half-metallic state of the manganites, the needed *p*-wave superconductivity in the system is induced undoubtedly due to the proximity effect [3.28–3.31]. The key feature of these heterostructures is the magnitude of the proximity induced triplet superconducting gap Δ_{tr}, i. e., *the magnitude of the topological pairing gap*. In manganite nanoparticles, this gap will be more than three times larger than the largest gap among *s*-wave SCs – the $\Delta(\sigma)$ gap MgB_2 [3.104]. Therefore, we believe that the manganite $(La_{1-x}R_x)MnO_3$ nanoparticles depositing on a *s*-wave SC are the most promising materials where *high-temperature topological superconducting states* can be realized. However, to our best knowledge, these systems are not yet studied in detail.

3.9 Conclusion

Systematic character and repeatability of the key experimental observations that have been detected by the point-contact Andreev reflection spectroscopy on the superconductor-half-metallic manganite heterostructures identify some general physical phenomena in transport properties of proximity coupled singlet superconductor-half-metallic manganite nanostructures. It was found that superconductor–half-metallic manganite hybrids provide an experimental possibility to accomplish artificial materials where a topologically nontrivial superconducting state and Majorana fermions can be realized. The basic factor of these conclusions is a local (fluctuated) high-temperature triplet superconductivity in half-metallic manganites. Although the local gap amplitude is large, there is no phase stiffness, and the system is incapable of displaying a

long-range superconducting state. Nonetheless, local phase rigidity survives and being proximity coupled to a superconductor, the long-range coherency is restored. The experimental evidence of the latent spin-triplet superconductivity in half-metal manganites allows to design an experimentally accessible way for overcoming bottleneck of spin-triplet pairing induced in proximitized structures of spin-singlet superconductors with time-reversal symmetry breaking counterparts and opens a new framework in topological superconductivity. Further experimental and theoretical works are needed to prove (or disprove) this platform for engineering topological superconductors and Majorana fermions.

The authors thank M. Belogolovskii for stimulating discussions and reading the manuscript.

3.10 References to chapter 3

3.1 Žutić I., Fabian J., Das Sarma S. Spintronics: Fundamentals and applications. *Rev. Mod. Phys*. 2004. V. 76. P. 323–410.

3.2 Anders S., Blamire M. G., Buchholz F.-Im., Crété D.-G., Cristiano R., Febvre P., Fritzsch L., Herr A., Il'ichev E., Kohlmann J., Kunert J., Meyer H.-G., Niemeyer J., Ortlepp T., Rogalla H., Schurig T., Siegel M., Stolz R., Tarte E., ter Brake H. J. M., Toepferm H., Villegier J.-C., Zagoskin A. M., Zori A. B. European roadmap on superconductive electronics – status and perspectives. *Physica C*. 2010. V. 470. P. 2079–2126.

3.3 Tao Y. C., Hu J. G. Superconducting spintronics: Spin-polarized transport in superconducting junctions with ferromagnetic semiconducting contact. *J. Appl. Phys*. 2010. V. 107. P. 041101.

3.4 Linder J., Robinson J. W. A. Superconducting spintronics. *Nature Phys.* 2015. V. 11. P. 307–315.

3.5 Eschrig M. Spin-polarized supercurrents for spintronics: a review of current progress. *Rep. Prog. Phys*. 2015. V. 78. P. 104501.

3.6 Yang G., Ciccarelli Ch., Robinson W. A. Boosting spintronics with superconductivity. *APL Mater*. 2021. V. 9. P. 050703.

3.7 Golovchanskiy I. A., Abramov N. N., Stolyarov V. S., Bolginov V. V., Ryazanov V. V., Golubov A. A., Ustinov A. U. Ferromagnet / Supercon-

ductor Hybridization for Magnonic Applications. *Adv. Funct. Mater.* 2018. V. 28. P. 1802375.

3.8 Alicea J. New directions in the pursuit of Majorana fermions in solid state systems. *Rep. Prog. Phys.* 2012. V. 75. P. 076501.

3.9 Beenakker C. W. J. Search for Majorana Fermions in Superconductors. *Annu. Rev. Condens. Matter Phys.* 2013. V. 4. P. 113–136.

3.10 Sato M., Ando Y. Topological superconductors: a review. *Rep. Prog. Phys.* 2017. V. 80. P. 076501.

3.11 Balatsky A. V., Vekhter I., Zhu J.-X. Impurity-induced states in conventional and unconventional superconductors. *Rev. Mod. Phys.* 2006. V. 78. P. 373–433.

3.12 Kitaev A. Fault-tolerant quantum computation by anyons. *Ann. Phys.* 2003. V. 303. P. 2–30.

3.13 Freedman M. H., Kitaev A., Larsen M. J., Wang Z. Topological quantum computation. *Bull. Am. Math. Soc.* 2003. V. 40. P. 31–38.

3.14 Knapp C., Zaletel M., Liu D. E., Cheng M., Bonderson P., Nayak C. The nature and correction of diabatic errors in anyon braiding. *Phys. Rev. X.* 2016. V. 6. P. 041003.

3.15 Nayak C., Simon S. H., Stern A., Freedman M., Das Sarma S. Non-Abelian anyons and topological quantum computation. *Rev. Mod. Phys.* 2008. V. 80. P. 1083–1159.

3.16 Plugge S., Rasmussen A., Egger R., Flensberg K. Majorana box qubits. *New J. Phys.* 2017. V. 19. P. 012001.

3.17 Choy T.-P., Edge J. M., Akhmerov A. R., Beenakker C. W. J. Majorana fermions emerging from magnetic nanoparticles on a superconductor without spin-orbit coupling. *Phys. Rev. B.* 2011. V. 84. P. 195442.

3.18 Chung S. B., Zhang H.-J., Qi X.-L., Zhang S.-Ch. Topological superconducting phase and Majorana fermions in half-metal / superconductor heterostructures. *Phys. Rev. B.* 2011. V. 84. P. 060510(R).

3.19 Nadj-Perge S., Drozdov I. K., Bernevig B. A., Yazdani A. Proposal for realizing Majorana fermions in chains of magnetic atoms on a superconductor. *Phys. Rev. B.* 2013. V. 88. P. 020407(R).

3.20 Gorczyca-Goraj A., Domański T., Maśka M. M. Topological superconductivity at finite temperatures in proximitized magnetic nanowires. *Phys. Rev. B.* 2019. V. 99. P. 235430.

3.21 Crawford D., Mascot E., Morr D. K., Rachel S. High-temperature Majorana fermions in magnet-superconductor hybrid systems. *Phys. Rev. B*. 2020. V. 101. P. 174510.
3.22 Kasai M., Ohno T., Kanke Y, Kozono Y., Hanazono M., and Sugita Y. Current-Voltage Characteristics of $YBa_2Cu_3O_y$ $La_{0.7}Ca_{0.3}MnO_z/YBa_2Cu_3O_y$ trailered-type junctions. *Jpn. J. Appl. Phys*. 1990. V. 29. P. L2219–L2222.
3.23 Kasai M., Kanke Y., Ohno T., Kozono Y. Possible mechanism of proximity effect coupled to spin fluctuation in YBa_2Cu_3Oy/magnetic manganese oxide/$YBa_2Cu_3O_y$ junctions. *J. Appl. Phys*. 1992. V. 72. P. 5344–5349.
3.24 Kalcheim Y., Kirzhner T., Koren G., Millo O. Long-range proximity effect in $La_{2/3}Ca_{1/3}MnO_3$/(100)$YBa_2Cu_3O_{7-\delta}$ ferromagnet / superconductor bilayers: Evidence for induced triplet superconductivity in the ferromagnet. *Phys. Rev. B*. 2011. V. 83. P. 064510.
3.25 Visani C., Sefrioui Z., Tornos J., Leon C., Briatico J., Bibes M., Barthélémy A., Santamaría J., Villegas J. E. Equal-spin Andreev reflection and long-range coherent transport in high-temperature superconductor / half-metallic ferromagnet junctions. *Nat. Phys*. 2012. V. 8. P. 539–543.
3.26 Eschrig M., Löfwander T. Triplet supercurrents in clean and disordered half-metallic ferromagnets. *Nat. Phys*. 2008. V. 4. P. 138–143.
3.27 D'yachenko A. I., Krivoruchko V. N., Tarenkov V. Yu. Andreev spectroscopy of point contacts between a low-temperature superconductor and manganite. *Fiz. Nizk. Temp*. 2006. V. 32. P. 1085–1095. [*Low Temp. Phys*. 2006. V. 32. P. 824–831].
3.28 Krivoruchko V. N., Tarenkov V. Yu. Local triplet superconductivity of $La_{0.65}Ca_{0.35}MnO_3$-X point contacts (X = Pb, MgB_2). *Phys. Rev. B*. 2007. V. 75. P. 214508.
3.29 Krivoruchko V. N., Tarenkov V. Yu. Anomalous superconductivity of Pb/$La_{0.7}Sr_{0.3}MnO_3$ point contacts. *Phys. Rev. B*. 2008. V. 78. P. 054522.
3.30 Krivoruchko V. N., Tarenkov V. Yu. Triple-gap superconductivity of MgB_2-(La,Sr)MnO_3 composite. *Phys. Rev. B*. 2012. V. 86. P. 104502.
3.31 Krivoruchko V. N., D'yachenko A. I., Tarenkov V. Yu. Andreev-spectroscopy study of unconventional superconductivity in MgB_2:(La,Sr)MnO_3

nanocomposite. *Fiz. Nizk. Temp.* 2014. V. 40. P. 1147–1154. [*Low Temp. Phys.* 2014. V. 40. P. 895–901].

3.32 Krivoruchko V. N., Dyachenko A. I., Tarenkov V. Y. Point-contact Andreev-reflection spectroscopy of doped manganites: Charge carrier spin-polarization and proximity effects (Review Article). *Fiz. Nizk. Temp*. 2013. V. 39. P. 276–292. [*Low Temp. Phys.* 2013. V. 39. P. 211–224].

3.33 D'yachenko A. I., Tarenkov V. Yu., Krivoruchko V. N. The Berezinskii–Kosterlitz–Thouless transition in bulk MgB_2:(La,Sr)MnO_3 superconductor-ferromagnetic nanocomposites. *Fiz. Nizk. Temp.* 2019. V. 45. 1360–1365. [*Low. Temp. Phys.* 2019. V. 45. 1156–1160].

3.34 Krivoruchko V. N., Tarenkov V. Yu. Percolation transitions in d-wave superconductor-half-metallic ferromagnet nanocomposites. *Fiz. Nizk. Temp.* 2019. V. 45. P. 555–561. [*Low. Temp. Phys.* 2019. V. 45. P. 476–481].

3.35 D'yachenko A. I., Krivoruchko V. N., Tarenkov V. Yu. Two-dimensional Berezinskii–Kosterlitz–Thouless topological phase transition in three-dimensional $Bi_2Sr_2Ca_2Cu_3O_{6+x}$:(La,Sr)MnO_3 nanocomposites. *Fiz. Nizk. Temp.* 2021. V. 47. P. 501–508. [*Low Temp. Phys*. 2021. V. 47. P. 466–472].

3.36 Krivoruchko V. N. Local spin-triplet superconductivity in half-metallic manganites: A perspective platform for high-temperature topological superconductivity. *Fiz. Nizk. Temp*. 2021. V. 47. P. 891–988. [*Low Temp. Phys*. 2021. V. 47. P. 901–907].

3.37 Giroud M., Courtois H., Hasselbach K., Mailly D., Pannetier B. Superconducting proximity effect in a mesoscopic ferromagnetic wire. *Phys. Rev. B.* 1998. V. 58. P. R11872–R11875.

3.38 Petrashov V. T., Sosnin I. A., Cox I., Parsons A., Troadec C. Giant Mutual Proximity Effects in Ferromagnetic / Superconducting Nanostructures. *Phys. Rev. Lett.* 1999. V. 83. P. 3281–3284.

3.39 Lawrence M. D., Giordano N. Proximity effects in superconductor-ferromagnet junctions. *J. Phys.: Condens. Matter*. 1999. V. 11. P. 1089–1084.

3.40 Kalcheim Y., Millo O., Egilmez M., Robinson J. W. A., Blamire M. G. Evidence for anisotropic triplet superconductor order parameter in half-metallic ferromagnetic $La_{0.7}Ca_{0.3}Mn_3O$ proximity coupled to superconducting $Pr_{1.85}Ce_{0.15}CuO_4$. *Phys. Rev. B.* 2012. V. 85. P. 104504.
3.41 Keizer R. S., Goennenwein S. T. B., Klapwijk T. M., Maio G., Xiao G., Gupta A. A spin triplet supercurrent through the half-metallic ferromagnet CrO_2. *Nature (London).* 2006. V. 439. P. 825–827.
3.42 Sosnin I., Cho H., Petrashov V., Volkov A. F. Superconducting Phase Coherent Electron Transport in Proximity Conical Ferromagnets. *Phys. Rev. Lett.* 2006. V. 96. P. 157002.
3.43 Buzdin A. I. Proximity effects in superconductor-ferromagnet heterostructures. *Rev. Mod. Phys.* 2005. V. 77. P. 935–976.
3.44 Kadigrobov A., Skekhter R. I., Jonson M. Quantum spin fluctuations as a source of long-range proximity effects in diffusive ferromagnet-super conductor structures. *Europhys. Lett.* 2001. V. 54. P. 394–400.
3.45 Bergeret F. S., Volkov A. F., Efetov K. B. Odd triplet superconductivity and related phenomena in superconductor-ferromagnet structures. *Rev. Mod. Phys*. 2005. V. 77. P. 1321–1373.
3.46 Deutscher G. Percolation and Superconductivity pp. 95–113. In book: Percolation, Localization and Superconductivity. Ed. Goldman A. B., Wolf S. A. Plenum: New York. 1984.
3.47 Skvortsov M. A., Larkin A. I., Feigel'man M. V. Proximity Action theory of superconductive nanostructures. *Usp. Fiz. Nauk* (Suppl.). 2001. V. 171. P. 76–80.
3.48 Sternfeld I., Shelukhin V., Tsukernik A., Karpovski M., Gerber A., Palevski A. Proximity effect in granular superconductor–normal metal structures. *Phys. Rev. B.* 2005. V. 71. P. 064515.
3.49 Andreev A. F. The Thermal conductivity of the intermediate state in superconductors. *Sov. Phys. JETP*. 1964. V. 19. P. 1228–1231.
3.50 Tokuyasu T., Sauls J. A., Rainer D. Proximity effect of a ferromagnetic insulator in contact with a superconductor. *Phys. Rev. B.* 1988. V. 38. P. 8823–8833.
3.51 Eschrig M. Spin-polarized supercurrents for spintronics. *Phys. Today*. 2011. V. 64. P. 43–49.

3.52 Dagotto E., Hotta T., Moreo A. Colossal magnetoresistant materials: the key role of phase separation. *Phys. Rep.* 2001. V. 344. P. 1–153.
3.53 Ziese M. Extrinsic magnetotransport phenomena in ferromagnetic oxides. *Rep. Prog. Phys.* 2002. V. 65. P. 143–249.
3.54 Krivoruchko V. N. The Griffiths phase and the metal-insulator transition in substituted manganites (Review Article). *Fiz. Nizk. Temp.* 2014. V. 40. P. 756–774. [Low Temp. Phys. 2014. V. 40. P. 586–599].
3.55 Zener C. Interaction between the d-shells in the transition metals. II. Ferromagnetic compounds of manganese with perovskite structure. *Phys. Rev.* 1951. V. 82. P. 403–405.
3.56 de Groot R. A., Mueller F. M., van Engen P. G., Buschow K. H. J. New class of materials: half-metallic ferromagnets. *Phys. Rev. Lett.* 1983. V. 50. P. 2024–2027.
3.57 Bowen M., Bibes M., Barthélémy A., Contour J.-P., Anane A., Lemaître Y., Fert A. Nearly total spin polarization in $La_{2/3}Sr_{1/3}MnO_3$ from tunneling experiments. *Appl. Phys. Lett.* 2003. V. 82. P. 233–235.
3.58 Savosta M. M., Krivoruchko V. N., Danilenko I. A., Tarenkov V. Yu., Konstantinova T. E., Borodin A. V., Varyukhin V. N. Nuclear spin dynamics and magnetic structure of nanosized particles of $La_{0.7}Sr_{0.3}MnO_3$. *Phys. Rev. B.* 2004. V. 69. P. 024413.
3.59 Krivoruchko V., Konstantinova T., Mazur A., Prokhorov A., Varyukhin V. Magnetic resonances spectroscopy of nanosize particles $La_{0.7}Sr_{0.3}MnO_3$. *J. Magn. Magn. Mater*. 2006. V. 300. P. e122–e125.
3.60 Ulyanov A. N., Yang D. S., Mazur A. S., Krivoruchko V. N., Levchenko G. G., Danilenko I. A., Konstantinova T. E. Local structure and magnetic inhomogeneity of nano-sized $La_{0.7}Sr_{0.3}MnO_3$ manganites. *J. Appl. Phys.* 2011. V. 109. P. 123928.
3.61 Liu X., Panguluri R. P., Huang Z.-F., Nadgorny B. Double percolation transition in superconductor-ferromagnet nanocomposites. *Phys. Rev. Lett*. 2010. V. 104. P. 035701.
3.62 Acharya S., Biswal A. K., Ray J., Vishwakarma P. N. Study of $Bi_2Sr_2CaCu_2O_8$/ $BiFeO_3$ nano-composite for electrical transport applications. *J. Appl. Phys.* 2012. V. 112. P. 053916.

3.63 Strelniker Y. M., Frydman A., Havlin S. Percolation model for the superconductor-insulator transition in granular films. *Phys. Rev. B.* 2007. V. 76. P. 224528.
3.64 Sternfeld I., Shelukhin V., Tsukernik A., Karpovski M., Gerber A., Palevski A. Proximity effect in granular superconductor–normal metal structures. *Phys. Rev. B.* 2005. V. 71. P. 064515.
3.65 Ruiz-Valdepeñas L., Vélez M., Valdés-Bango F., Álvarez-Prado L. M., Martín J. I., Navarro E., Alameda J. M., Vicent J. L. Double percolation effects and fractal behavior in magnetic / superconducting hybrids. *New J. Phys.* 2013. V. 15. P. 103025.
3.66 Berezinsky V. L. Destruction of long-range order in one-dimensional and two-dimensional systems having a continuous symmetry group. I. Classical systems. *JETP*. 1971. V. 59. P. 907–920. [*Sov. Phys. JETP*. 1971. V. 32. P. 493–500].
3.67 Kosterlitz J. M., Thouless D. J. Ordering, metastability and phase transitions in two-dimensional systems. *J. Phys. C.* 1973. V. 6. P. 1181–1203.
3.68 Kosterlitz J. M. The critical properties of the two-dimensional xy model. *J. Phys. C.* V. 7. P. 1046–1060.
3.69 Blatter G., Feigel'man M. V., Geshkenbein V. B., Larkin A. I., Vinokur V. M. Vortices in high-temperature superconductors. *Rev. Mod. Phys.* 1994. V. 66. P. 1125–1388.
3.70 Goldman A. M. The Berezinskii–Kosterlitz–Thouless transition in superconductors. in 40 Years of Berezinskii–Koste–Rlitz–Thouless Theory. Ed. José J. V. World Scientific: Singapore. 2013.
3.71 Costa B. V., Lima A. B. Dynamical behavior of vortices in thin film magnetic systems. *J. Magn. Magn. Mater.* 2012. V. 324. P. 1999–2005.
3.72 Tutsch U., Wolf B., Wessel S., Postulka L., Tsui Y., Jeschke H. O., Opahle I., Saha-Dasgupta T., Valentí R., Brühl A., Remović-Langer K., Kretz T., Lerner H.-W., Wagner M., Lang M. Evidence of a field-induced Berezinskii–Kosterlitz–Thouless scenario in a two-dimensional spin–dimer system. *Nat. Commun.* 2014. V. 5. P. 5169.
3.73 Minnhagen P. The two-dimensional Coulomb gas, vortex unbinding, and superfluid-superconducting films. *Rev. Mod. Phys*. 1987. V. 59. P. 1001–1066.

3.74 Ashoka A., Bhagyashree K. S., Bhat S. V. Signatures of field-induced Berezinskii–Kosterlitz–Thouless correlations in the three-dimensional manganite $Bi_{0.5}Sr_{0.5}Mn_{0.9}Cr_{0.1}O_3$. *Phys. Rev. B.* 2020. V. 102. P. 024429.
3.75 Benfatto L., Castellani C., Giamarchi T. Doping dependence of the vortex-core energy in bilayer films of cuprates. *Phys. Rev. B.* 2008. V. 77. P. 100506(R).
3.76 Benfatto L., Castellani C., Giamarchi T. Broadening of the Berezinskii–Kosterlitz–Thouless superconducting transition by inhomogeneity and finite-size effects. *Phys. Rev. B.* 2009. V. 80. P. 214506.
3.77 Gantmakher V. F. Localized superconducting pairs. *Fiz. Nizk. Temp.* 2011. V. 37. P. 71–83. [*Low Temp. Phys.* 2011. V. 37. P. 59–68].
3.78 Resnick D. J., Garland J. C., Boyd J. T., Shoemaker S., Newrock R. S. Kosterlitz-Thouless transition in proximity-coupled superconducting arrays. *Phys. Rev. Lett.* 1981. V. 47. 1542–1545.
3.79 Halperin B. I., Nelson D. R. Resistive transition in superconducting films. *J. Low Temp. Phys*. 1979. V. 36. P. 599–616.
3.80 Doniach S., Huberman B. A. Topological Excitations in Two-dimensional superconductors. *Phys. Rev. Lett.* 1979. V. 42. P. 1169–1172.
3.81 Bergeret F. S., Virtanen P., Ozaeta A., Heikkilä T. T., Cuevas J. C. Supercurrent and Andreev bound state dynamics in superconducting quantum point contacts under microwave irradiation. *Phys. Rev. B.* 2011. V. 84. P. 054504.
3.82 Semenov A. V., Devyatov I. A., de Visser P. J., Klapwijk T. M. Coherent excited states in superconductors due to a microwave field. *Phys. Rev. Lett*. 2016. V. 117. P. 047002.
3.83 Kirkpartrick S. Percolation and conduction. *Rev. Mod. Phys.* 1973. V. 45. P. 574–588.
3.84 Bunde A., Dieterich W. Percolation in composites. *J. Electroceram*. 2000. V. 5. P. 81–92.
3.85 Balberg I. Tunnelling and percolation in lattices and the continuum. *J. Phys. D: Appl. Phys.* 2009. V. 42. P. 064003.
3.86 Niu Z. P., Xing D. Y. Spin-triplet pairing states in ferromagnet / ferromagnet / d-Wave superconductor heterojunctions with noncollinear magnetizations. *Phys. Rev. Lett.* 2007. V. 98. P. 057005.

3.87 Hu T., Xiao H., Visani C., Sefrioui Z., Santamaria J., Almasan C. C. Evidence from magnetoresistance measurements for an induced triplet superconducting state in $La_{0.7}Ca_{0.3}MnO_3/YBa_2Cu_3O_{7-\delta}$ multilayers. *Phys. Rev. B.* 2009. V. 80. P. 060506(R).

3.88 Dybko K., Werner-Malento K., Aleshkevych P., Wojcik M., Sawicki M., Przyslupski P. Possible spin-triplet superconducting phase in the $La_{0.7}Sr_{0.3}MnO_3/YBa_2Cu_3O_7/La_{0.7}Sr_{0.3}MnO_3$ trilayer. *Phys. Rev. B.* 2009. V. 80. P. 144504.

3.89 Kalcheim Yo., Kirzhner T., Koren G., Millo O. Long-range proximity effect in $La_{2/3}Ca_{1/3}MnO_3/(100)YBa_2Cu_3O_{7-\delta}$ ferromagnet / superconductor bilayers: Evidence for induced triplet superconductivity in the ferromagnet. *Phys. Rev. B.* 2011. V. 83. P. 064510.

3.90 Wang W., Shao D. F., Xiao R. C., Lu W. J., Wu H. Y. Long-range spin-triplet superconductivity induced by magnetic field in d wave superconductor / ferromagnet hybrid system. *J. Supercond. Nov. Magn*. 2016. V. 29. P. 1741–1746.

3.91 Loktev V. M., Quick R. M., Sharapov S. G. Phase fluctuations and pseudogap phenomena. *Phys. Rep.* 2001. V. 349. P. 1–123.

3.92 Emery J. V., Kivelson S. A. Superconductivity in bad metals. *Phys. Rev. Lett.* 1995. V. 74. P. 3253–3256.

3.93 Berg E., Orgad D., Kivelson S. A. Route to high-temperature superconductivity in composite systems. *Phys. Rev. B.* 2008. V. 78. P. 094509.

3.94 Mondal M., Kamlapure A., Chand M., Saraswat G., Kumar S., Jesudasan J., Benfatto L., Tripathi V., Raychaudhuri P. Phase fluctuations in a strongly disordered s-wave NbN superconductor close to the metal-insulator transition. *Phys. Rev. Lett*. 2011. V. 106. P. 047001.

3.95 Sacépé B., Dubouchet T., Chapelier C., Sanquer M., Ovadia M., Shahar D., Feigel'man M., Ioffe L. Localization of preformed Cooper pairs in disordered superconductors. *Nature Phys*. 2011. V. 7. P. 239–244.

3.96 Blonder G. E., Tinkham M., Klapwijk T. M. Transition from metallic to tunneling regimes in superconducting microconstrictions: Excess current, charge imbalance, and supercurrent conversion. *Phys. Rev. B.* 1982. V. 25. P. 4515–4532.

3.97 Daghero D., Gonnelli R. S. Probing multiband superconductivity by point-contact spectroscopy. *Supercond. Sci. Technol.* 2010. V. 23. P. 043001.
3.98 Naidyuk Yu. G., Yanson I. K. Point-contact spectroscopy. Springer. 2005.
3.99 Pickett W. E., Singh D. J. Electronic structure and half-metallic transport in the $La_{1-x}Ca_xMnO_3$ system. *Phys. Rev. B.* 1996. V. 53. P. 1146–1160.
3.100 Wei J. Y. T., Yeh N.-C., Vasquez R. P. Tunneling evidence of half-metallic ferromagnetism in $La_{0.7}Ca_{0.3}MnO_3$. *Phys. Rev. Lett.* 1997. V. 79. P. 5150–5153.
3.101 Jo M.-H., Mathur N. D., Todd N. K., Blamire M. G. Very large magnetoresistance and coherent switching in half-metallic manganite tunnel junctions. *Phys. Rev. B.* 2000. V. 61. P. R14905–R15908.
3.102 D'yachenko A. I., D'yachenko V. A., Tarenkov V. Yu., Krivoruchko V. N. Spin polarization of charge carriers and Andreev reflection in (LaCa)MnO / superconductor point contacts. *Fiz. Tverd. Tela.* 2006. V. 48. P. 407–414. [*Phys. Solid State.* 2006. V. 48. P. 432–440].
3.103 Dynes R. C., Narayanamurti V., Garno J. P. Direct Measurement of quasiparticle-lifetime broadening in a strong-coupled superconductor. *Phys. Rev. Lett.* 1978. V. 41. P. 1509–1512.
3.104 Xi X. X. Two-band superconductor magnesium diboride. *Rep. Prog. Phys.* 2008. V. 71. P. 116501.
3.105 Mitra J., Raychaudhuri A. K., Mukovskii Ya. M., Shulyatev D., Tokura Y., Hamada N. Depletion of the density of states at the Fermi level in metallic colossal magnetoresistive manganites. *Phys. Rev. B.* 2003. V. 68. P. 134428.
3.106 Saitoh T., Dessau D. S., Moritomo Y., Kimura T., Tokura Y., Hamada N. Temperature-dependent pseudogaps in colossal magnetoresistive oxides. *Phys. Rev. B.* 2000. V. 62. P. 1039–1043.
3.107 Tarenkov V. Yu., D'yachenko A. I., Krivoruchko V. N. Pressure-induced variation of the magnetic structure of the surface of $La_{0.6}Sr_{0.4}MnO_3$ granules. *Zh. Éksp. Teor. Fiz.* 2001. V. 120. P. 205–213. [*JETP*. 2001. V. 93. P. 180–187].
3.108 Edwards M. Ferromagnetism and electron-phonon coupling in the manganites. *Adv. Phys.* 2002. V. 51. P. 1259–1318.

3.109 Iguchi I., Yamaguchi T., Sugimoto A. Diamagnetic activity above Tc as a precursor to superconductivity in $La_{2-x}Sr_xCuO_4$ thin films. *Nature.* 2001. V. 412. P. 420–423.
3.110 González J. L., de Mello E. V. L. Theory of the diamagnetism above the critical temperature for cuprates. *Phys. Rev. B.* 2004. V. 69. P. 134510.
3.111 Eschrig M., Kopu J., Cuevas J. C., Schön G. Theory of half-metal / superconductor heterostructures. *Phys. Rev. Lett*. 2003. V. 90. P. 137003.
3.112 Bulaevskii L., Eneias R., Ferraz A. Triplet superconductivity in ferromagnets due to magnon exchange. *Phys. Rev. B.* 2019. V. 99. P. 064506.
3.113 Saitoh T., Dessau D. S., Moritomo Y., Kimura T. Temperature-dependent pseudogaps in colossal magnetoresistive oxides. *Phys. Rev. B.* 2000. V. 62. P. 1039.
3.114 Sau J. D., Tewari S., Lutchyn R. M., Stanescu T. D., das Sarma S. Non-Abelian quantum order in spin-orbit-coupled semiconductors: Search for topological Majorana particles in solid-state systems. *Phys. Rev. B.* 2010. V. 82. P. 214509.
3.115 Wimmer M., Akhmerov A. R., Dahlhaus J. P., Beenakker C. W. J. Quantum point contact as a probe of a topological superconductor. *New J. Phys.* 2011. V. 13. P. 053016.
3.116 Nakosai S., Tanaka Y., Nagaosa N. Two-dimensional p-wave superconducting states with magnetic moments on a conventional s-wave superconductor. *Phys. Rev. B.* 2013. V. 88. P. 180503(R).
3.117 Mourik V., Zuo K., Frolov S. M., Plissard S. R., Bakkers E. P. A. M., Kouwenhoven L. P. Signatures of Majorana fermions in hybrid superconductor-semiconductor nanowire devices. *Science*. 2012. V. 336. P. 1003–1007.
3.118 Das A., Ronen Y., Most Y., Oreg Y., Heiblum M., Shtrikman H. Zero-bias peaks and splitting in an Al–InAs nanowire topological superconductor as a signature of Majorana fermions. *Nat. Phys.* 2012. V. 8. P. 887–895.
3.119 Deng M. T., Yu C. L., Huang G. Y., Larsson M., Caroff P., Xu H. Q. Zero-bias peaks and splitting in an Al–InAs nanowire topological superconductor as a signature of Majorana fermions. *Nano Lett.* 2012. V. 12. P. 6414–6419.

3.120 Liu J., Potter A. C., Law K. T., Lee P. A. Zero-bias peaks in the tunneling conductance of spin-orbit-coupled superconducting wires with and without Majorana end-states. *Phys. Rev. Lett.* 2012. V. 109. P. 267002.
3.121 Pikulin D. I., Dahlhaus J. P., Wimmer M., Schomerus H., Beenakker C. W. J. A zero-voltage conductance peak from weak antilocalization in a Majorana nanowire. *New J. Phys.* 2012. V. 14. P. 125011.
3.122 Bagrets D., Altland A. Class D Spectral Peak in Majorana Quantum Wires. *Phys. Rev. Lett.* 2012. V. 109. P. 227005.
3.123 Liu C.-X., Sau J. D., Stanescu T. D., das Sarma S. Andreev bound states versus Majorana bound states in quantum dot-nanowire-superconductor hybrid structures: Trivial versus topological zero-bias conductance peaks. *Phys. Rev. B.* 2017. V. 96. P. 075161.
3.124 Kitaev A. Yu. Unpaired Majorana fermions in quantum wires. *Phys.-Usp.* 2001. V. 44. P. 131–136.